Transportation Research Part C 174 (2025) 105104

Contents lists available at ScienceDirect

Transportation Research Part C

journal homepage: www.elsevier.com/locate/trc

Multi-element probabilistic collocation solution for dynamic continuum pedestrian models with random inputs

Zepeng Liu [a], S.C. Wong [b,*], Liangze Yang [c], Chi-Wang Shu [d], Mengping Zhang [a]

[a] School of Mathematical Sciences, University of Science and Technology of China, Hefei, Anhui 230026, China
[b] Department of Civil Engineering, The University of Hong Kong, Hong Kong, China
[c] School of Mathematical Sciences, Anhui University, Hefei, Anhui, 230601, China
[d] Division of Applied Mathematics, Brown University, Providence, RI 02912, USA

ARTICLE INFO

Keywords:
Pedestrian dynamics
Dynamic continuum modeling
Demand stochasticity
Polynomial chaos expansions
Multi-element probabilistic collocation method

ABSTRACT

This study focuses on dynamic continuum pedestrian flow models with random inputs, which can be represented by sets of partial differential equations with some modeling parameters being randomized. Under random conditions, the model outputs are no longer fixed and may differ appreciably from their respective average levels. Simulating the resulting distribution is important as it helps quantify the effects of uncertainties on traffic behaviors when evaluating walking facilities. Through two examples based on continuum models, the effect of random inputs on pedestrian flow propagation is qualitatively analyzed. Crowd evacuation is found to be effective in reducing the variation and risk produced by randomness, while congestion is observed to significantly increase the uncertainty within the system. For a general system without an explicitly known exact solution, an existing efficient solver — the multi-element probabilistic collocation method (ME-PCM) — is introduced to derive the solution distribution numerically. The ME-PCM is non-intrusive and flexible and has no limitations in terms of governing partial differential equations and the numerical schemes for solving them. The ME-PCM's use of element-wise local orthogonal polynomials to represent the solution enables it to converge efficiently even if shocks occur during the modeling period. As a demonstration case, the well-known Hughes model is applied in a numerical example with a corridor and an obstacle. The demand at the inflow boundary is randomized to a lognormal distribution that represents day-to-day demand stochasticity. The results indicate that the ME-PCM's solution converges more rapidly than those of the Monte Carlo and generalized polynomial chaos methods. Statistical information on pedestrian density is derived from the ME-PCM solution and can be used to identify the locations in walking facilities where the average pedestrian density is moderate but where exceptional congestion with a large variance can occur. This successful application shows the possibility of quantifying the uncertainty in pedestrian flow models using the ME-PCM. The proposed approach can also be applied to models with other similar random inputs, given that a well-established algorithm for deterministic cases is available.

* Corresponding author.
E-mail addresses: lzp0375@mail.ustc.edu.cn (Z. Liu), hhecwsc@hku.hk (S.C. Wong), lzeyang@ahu.edu.cn (L. Yang), chi-wang_shu@brown.edu (C.-W. Shu), mpzhang@ustc.edu.cn (M. Zhang).

https://doi.org/10.1016/j.trc.2025.105104
Received 9 July 2024; Received in revised form 29 January 2025; Accepted 10 March 2025
Available online 19 March 2025

1. Introduction

Traffic flow is influenced by various stochastic factors, including external factors (e.g., weather conditions) and internal factors (e.g., transportation facilities, vehicle characteristics, and driver behaviors). For instance, more people typically enter underground stations on rainy days (Sumalee et al., 2011a), and the free-flow speed of drivers tends to decrease during severe rainstorms and other extreme weather conditions (Chung et al., 2005). Considering these stochastic influences in traffic flow modeling helps to accurately predict and further investigate dynamic evolution.

Recent studies have extensively investigated the incorporation of stochasticity into traffic flow modeling in the fields of vehicular and pedestrian flows. Wang and Papageorgiou (2005) presented a general stochastic macroscopic traffic flow model of freeway stretches based on a traffic state estimator. Sumalee et al. (2011b) and Zhong et al. (2013) proposed a first-order macroscopic stochastic cell transmission model, formulating each operational mode as a discrete time bilinear stochastic system to calculate the traffic density of freeway segments under demand and supply uncertainties. In addition to randomizing the density function, researchers have attempted to quantify the stochasticity in fundamental diagrams and the corresponding phase transitions by randomizing the relationships among flow, density and velocity. For example, Li et al. (2012) incorporated a stochastic fundamental diagram into their modified Lighthill–Whitham–Richards (LWR) model, and Jabari et al. (2014) derived a stochastic relationship between macroscopic variables based on Newell's simplified car-following model. Other studies have explored the randomization of driving behaviors and road capacity. For example, Fan et al. (2023) investigated the stochasticity of the LWR model arising from driver heterogeneity by randomizing free-flow speed. Brilon et al. (2005) introduced a realistic and useful concept of stochastic capacities, which was then used to identify the characteristics of traffic flow breakdown and occurrence conditions (Kerner and Klenov, 2006; Kesting et al., 2010). Additionally, recent research has aimed at modeling pedestrian flow from the perspective of game theory. Dogbé (2010) and Lachapelle and Wolfram (2011) applied mean-field game (MFG) theory to examine the motion and congestion of pedestrian crowd dynamics. Burger et al. (2013) and Djehiche et al. (2017) investigated the evacuation of pedestrians based on the MFG approach. Barreiro-Gomez and Masmoudi (2023) studied crowd dynamics in both non-atomic and atomic differential games and showed the connection of their game-theoretical models with Hughes model and the LWR traffic model. Ghattassi and Masmoudi (2023) presented a generalization of Hughes model based on MFGs, considering pedestrian behaviors that avoid high-density regions. Furthermore, Tordeux and Schadschneider (2016) introduced stochastic noise into optimal velocity models for pedestrians, resulting in the emergence of stop-and-go waves. Ramírez et al. (2019) implemented a cellular automaton model to investigate random interactions among pedestrians, parameterizing social, cultural, and psychological behaviors as sources of randomness.

This study considers macroscopic dynamic continuum pedestrian flow models, which are written as partial differential equations. The continuum modeling approach places a greater focus on the collective and average behavior of pedestrians, and it offers a robust theoretical description of observable phenomena, such as shock formation and evolution, providing valuable insights for an analytical understanding of the issue (Liang et al., 2021; Huang et al., 2009a). Moreover, it reduces the problem size and saves considerable computation time in the case of crowd simulation under high-density conditions and long-term planning (Cao et al., 2015), especially for uncertainty quantification which typically requires repeatedly solving the model. In a deterministic case, the model inputs, including relation parameters and initial boundary conditions, are determined, and an algorithm is then used to derive the output (solution). However, uncertainty is always present in the model inputs, as a determined set of inputs and outputs has difficulty representing all possible scenarios. If the inputs are randomized based on realistic observation, the output is no longer determined and varies in a range that may be different from the average level. For example, the traffic demand at the entrance of a platform varies across different days and can be considered as a random input influenced by a scaling parameter in what is termed day-to-day demand stochasticity. The scaling parameter is assumed to follow a certain distribution, leading to the pedestrian density varying within a range. Modeling demand stochasticity is important, as it can be utilized in designing walking facilities by identifying critical locations that arise from varying demand distributions on different days. There may be instances where the average density at certain locations is moderate, but with a large variance, leading to exceptional congestion on critical days that can be overlooked during the standard design process based on average demand. Moreover, the likelihood of such critical situations can be quantified, allowing for a trade-off between the operational performance and construction cost. By adopting the probability distribution derived from stochastic modeling, the parameters of walking facilities, such as the corridor width and platform area, can be designed using a critical probability threshold, such as the 95% percentile value, ensuring that the system fails only 5% of the time during operation.

Under random model inputs, this study derives the distribution of pedestrian flow characteristic variables in an efficient way. The commonly used Monte Carlo (MC) method is useful for its robustness. When combined with high-order numerical schemes for deterministic partial differential equations (PDEs), the MC method has proven successful in addressing various stochastic vehicular problems (Parry and Hazelton, 2013; Sayegh et al., 2018; Fan et al., 2023). In most cases, a large sample size is necessary to obtain accurate estimates of statistical properties, such as the mean and standard deviation, as the MC method has only a half-order convergence rate. Some techniques, such as the adoption of a quasi-random sequence (Caflisch, 1998) and the multilevel MC method (Giles, 2015), can be used to enhance computational efficiency, but they are computationally expensive. In addition to statistical MC methods, several nonstatistical approaches have been proposed (Wiener 1938, Xiu and Karniadakis 2002, Wan and Karniadakis 2005, Cheng et al. 2013a,b). One such approach is based on polynomial chaos (Wiener, 1938), using orthogonal polynomial functions to represent the stochastic process, and has proven effective for certain problems (Ghanem and Red-Horse, 1999; Ghanem and Spanos, 2003). Xiu and Karniadakis (2002) proposed the generalized polynomial chaos (gPC) strategy and highlighted that the type of orthogonal polynomial should correspond to the stochastic process and distribution to achieve optimal

exponential convergence. Compared with MC methods, such a spectral method provides a better convergence rate and thus has a reduced computational cost. The method uses a truncated expansion for the solution, and the expansion coefficients can be determined by adopting stochastic Galerkin (SG) methods. In gPC-SG methods, truncated expressions are substituted into the original PDEs, and a new group of equations is derived from the coefficients in the expansion.

However, difficulties arise when applying spectral methods to pedestrian flow models with random inputs. First, the governing equations in pedestrian flow models are typically non-linear, and the gPC method thus makes the problem deterministic but without holding the original equation properties. A well-known example is the hyperbolic mass conservation equation. After the gPC procedure, the equation sets for expansion coefficients are no longer hyperbolic. Second, congestion is observed during the period, and the locations where shock appears may differ with random inputs, leading to a sharp jump or discontinuity in the randomized parameter space. In this situation, convergence cannot be ensured by adopting a global polynomial basis and typical gPC methods.

To efficiently obtain the pedestrian density distribution, this study considers a multi-element probabilistic collocation method (ME-PCM) (Wan and Karniadakis, 2005, 2006; Foo et al., 2008) and shows that this avoids the above difficulties. As a foundational model, Hughes model (Hughes, 2002) provides a systematic framework for the dynamic macroscopic modeling of pedestrian flow problems, and many continuum models have been developed based on it. To illustrate the wide applicability of the ME-PCM and its attractive feature of having no restrictions on the equations and numerical schemes used, this study uses the representative Hughes model in a test on a numerical example with a corridor and obstacle as a first demonstration. The demand at the inflow boundary is randomized to a lognormal distribution that represents day-to-day demand stochasticity. From the ME-PCM solutions, the statistical pedestrian density information can be derived to evaluate walking facilities, considering the risk of exceptional congestion. To the best of the authors' knowledge, no prior study has investigated pedestrian flow stochasticity using this approach. This application of the spectral method offers a promising way to quantify the uncertainty in pedestrian traffic flow models. This paper provides a detailed framework of the ME-PCM. The method is shown to be robust and effective, especially for nonlinear problems such as those of demand stochasticity considered in the section reporting numerical results. Compared with MC methods, the ME-PCM has a much better convergence rate and computational efficiency. This study shows that the ME-PCM is a useful tool for quantifying uncertainties in macroscopic dynamic continuum pedestrian flow models without limitations on the PDEs used and the numerical schemes for solving them. The mathematical functions provided by the ME-PCM enable analytical analyses of key parameters in the model, including statistical quantities and sensitivity coefficients (Xiu, 2009; Foo et al., 2008). In addition, the ME-PCM can be applied to similar models with random inputs, given that a well-established algorithm for deterministic cases is available.

The remainder of this paper is structured as follows. Section 2 presents dynamic continuum models with random inputs in a general form, describes the analysis of the qualitative effect of random inputs on pedestrian flow propagation through two examples, and then outlines the algorithm application procedure for the ME-PCM, including the decomposition, sampling, and reconstruction steps. Section 3 details the adoption of the Hughes model with day-to-day demand stochasticity to demonstrate the effectiveness of the ME-PCM. Additionally, high-order finite-difference schemes are reviewed to solve deterministic PDEs. Numerical examples and simulation results, including density distribution plots, convergence rates, and a speedup comparison, are presented. Section 4 presents the concluding remarks.

2. Models and solution methods

2.1. Pedestrian flow models with random inputs

This study considers macroscopic dynamic continuum pedestrian flow models, which can be generally described as a set of time-dependent PDEs with initial boundary conditions; i.e.,

$$\partial_t \boldsymbol{U}(\boldsymbol{x},t) + \mathcal{L}(\boldsymbol{U}(\boldsymbol{x},t)) = 0, \qquad \forall(\boldsymbol{x},t) \in D \times (0,T], \tag{1a}$$

$$\boldsymbol{U}(\boldsymbol{x},0) = \boldsymbol{U}^0(\boldsymbol{x}), \qquad \forall \boldsymbol{x} \in D, \tag{1b}$$

$$\boldsymbol{U}(\boldsymbol{x},t) = \boldsymbol{G}(t), \qquad \forall(\boldsymbol{x},t) \in \partial D \times (0,T]. \tag{1c}$$

Here, D is a two-dimensional walking facility domain and ∂D is the boundary of D. $t \in (0,T], T > 0$ is time, and $\boldsymbol{x} = (x,y)$ denotes spatial coordinates. The components of $\boldsymbol{U}(\boldsymbol{x},t)$ represent time-varying pedestrian flow characteristic variables, such as density and velocity. The time-dependent governing equations are given as (1a), where $\mathcal{L}$ is the spatial operator representing different kinds of dynamic continuum models, including but not limited to the models of Hughes (2002), Huang et al. (2009b), Xia et al. (2009) and Hoogendoorn and Bovy (2004), and other first-order and second-order pedestrian flow models that can be written as partial differential equations. Given the initial condition (1b) and boundary condition (1c), the above system is closed as a deterministic system and can be solved using a number of numerical approaches, such as the adoption of finite difference and finite element schemes.

We assume that some parameters in the pedestrian flow model are randomized, and with different parameters, the output (solution) of the model may also have appreciable differences. Such randomized parameters are regarded as random inputs of the model and are assumed to follow certain distributions. For different problems, the randomness can enter the system from operator $\mathcal{L}$ in PDEs, from the initial conditions $\boldsymbol{U}^0$ and boundary conditions $\boldsymbol{G}$, and even from the geometry settings D and ∂D.

For simplicity, this study considers that the dimension of random inputs is one and a single random variable is appended to the generalized system. Consider a complete probability space $(\Omega, \mathcal{F}, \mathbb{P})$, where Ω is the sample space, $\mathcal{F}$ is the σ-algebra of subsets of

the random event ω, and $\mathbb{P}$ is a probability measure. Assume the input can be expressed as a random variable $\xi(\omega) : \Omega \mapsto \mathbb{R}$, with a probabilistic density function (PDF) $w(\xi)$. Let Θ be the image of $\xi(\Omega)$. The model with a random input is then expressed as

$$\partial_t \boldsymbol{U}(\boldsymbol{x}, t, \xi) + \mathcal{L}(\boldsymbol{U}(\boldsymbol{x}, t, \xi)) = 0, \qquad \forall (\boldsymbol{x}, t, \xi) \in D \times (0, T] \times \Theta, \tag{2a}$$

$$\boldsymbol{U}(\boldsymbol{x}, 0, \xi) = \boldsymbol{U}^0(\boldsymbol{x}, \xi), \qquad \forall (\boldsymbol{x}, \xi) \in D \times \Theta, \tag{2b}$$

$$\boldsymbol{U}(\boldsymbol{x}, t, \xi) = \boldsymbol{G}(t, \xi), \qquad \forall (\boldsymbol{x}, t, \xi) \in \partial D \times (0, T] \times \Theta. \tag{2c}$$

Here, the model is expressed in a general form to illustrate that the ME-PCM can be applied without limitations on governing PDEs and random inputs. Although different models can be considered, this study uses Hughes model (Hughes, 2002), on the basis of which many continuum models are developed, in a demonstration. The details are discussed in the section presenting the numerical example.

2.2. Qualitative effects of random inputs on pedestrian flow propagation

Two specific examples are used to demonstrate the continuum model's ability to analytically study pedestrian flow propagation within a stochastic paradigm. The continuum modeling approach provides a collective description of pedestrian traffic behaviors in an equation form, enabling the analytical analysis of pedestrian flow propagation with random inputs. For a system (2) in hyperbolic form which is commonly used in continuum models, the solution property and the influence of uncertainty can be mathematically studied (LeVeque, 1992; Schwab and Tokareva, 2013; Cho et al., 2014). For example, the shock formation in a traffic flow model can be explained using characteristic lines for hyperbolic systems (LeVeque, 1992). Accordingly, the qualitative effects of random inputs on pedestrian flow propagation are examined herein.

Consider a flow of pedestrians on a platform, where ρ and u denote the density and walking speed of the pedestrians, respectively. The density is restricted to $0 \le \rho \le \rho_{\max}$, where $\rho_{\max}$ is the maximum density. Because the pedestrian flow is conserved, the density and speed must satisfy the continuity equation

$$\rho_t + (\rho u)_x = 0. \tag{3}$$

The local walking speed $u = u(\rho)$ is related to the local density and can be determined using pedestrian fundamental diagrams. The Greenshields model yields the linear relation

$$u(\rho) = u_f(1 - \rho/\rho_{\max}), \tag{4}$$

where u_f is the free-flow speed of pedestrians. Substituting this term into (3) gives

$$\rho_t + f(\rho)_x = 0, \quad f(\rho) = \rho u_f(1 - \rho/\rho_{\max}). \tag{5}$$

Here, two types of initial and boundary conditions are considered. The randomness enters the system from the boundary condition in the first example, while the initial condition randomizes in the second example.

- **Example 1. Pedestrians marching into an empty platform.**

$$\partial_t \rho(x, t, \xi) + \partial_x f(\rho(x, t, \xi)) = 0, \qquad \forall (x, t, \xi) \in (0, L) \times (0, T] \times \Theta, \tag{6a}$$

$$\rho(x, 0, \xi) = 0, \qquad \forall (x, \xi) \in (0, L) \times \Theta, \tag{6b}$$

$$\rho(0, t, \xi) = \xi, \qquad \forall (t, \xi) \in (0, T] \times \Theta. \tag{6c}$$

  This model describes the state of pedestrians moving slowly from a queue ($x < 0$) to enter an empty field ($0 < x < L$), where L is the length of the platform. The parameter ξ here represents the density of the queue and is regarded as a random variable.

- **Example 2. Walking pedestrians meeting a jam.**

$$\partial_t \rho(x, t, \xi) + \partial_x f(\rho(x, t, \xi)) = 0, \qquad \forall (x, t, \xi) \in (-\infty, L) \times (0, T] \times \Theta, \tag{7a}$$

$$\rho(x, 0, \xi) = \xi, \qquad \forall (x, \xi) \in (-\infty, L) \times \Theta, \tag{7b}$$

$$\rho(L, t, \xi) = \rho_{\max}, \qquad \forall (t, \xi) \in (0, T] \times \Theta. \tag{7c}$$

  This model describes the state of walking pedestrians ($x < L$) meeting a jam at $x = L$. The parameter ξ here denotes the initial uniform density of the pedestrians and is again regarded as a random variable.

Using characteristic lines (LeVeque, 1992), the solution of these two examples at position x and time t can be determined based on the characteristic speed

$$f'(\rho) = u_f\left(1 - 2\rho/\rho_{\max}\right). \tag{8}$$

For the first example, if the random variable is assumed to be uniformly distributed, i.e., $\xi \sim \mathcal{U}(0, \rho_{max}/2)$, then the exact solution (Fig. 1(a)) is a rarefaction wave when $t < L/u_f$:

$$\rho(x, t, \xi) = \begin{cases} \xi, & 0 \le x < u_f t(1 - 2\xi/\rho_{\max}), \\ -\frac{\rho_{\max}}{2u_f t}\left(x - u_f t\right), & u_f t(1 - 2\xi/\rho_{\max}) \le x \le u_f t, \\ 0, & u_f t < x < L. \end{cases}$$

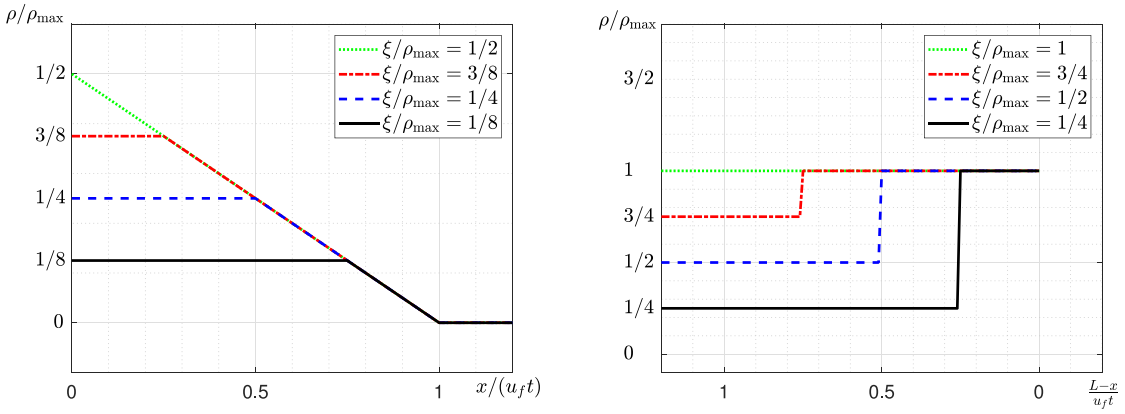

(a) Example 1: rarefaction solution. (b) Example 2: shock solution.

Fig. 1. The graphs of pedestrian density ρ in terms of location x for different inputs ξ. Left: result of example 1. Right: result of example 2.

By defining $\gamma = \frac{x}{u_f t}$, the solution can be expressed as

$$\rho(x,t,\xi) = \begin{cases} \xi, & 0 \le \gamma < 1 - 2\xi/\rho_{\max}, \\ -\frac{\rho_{\max}}{2}(\gamma - 1), & 1 - 2\xi/\rho_{\max} \le \gamma \le 1, \\ 0, & 1 < \gamma < L/(u_f t). \end{cases} \tag{9}$$

Notably, the exact solution (9) has three intervals. The interval $(0, 1-2\xi/\rho_{\max})$ represents the pedestrians still walking in the queue with a uniform speed $u(\xi)$. The interval $(1, L/(u_f t))$ represents the area that the pedestrians have not reached. The pedestrians in $(1-2\xi/\rho_{\max}, 1)$ begin to accelerate and spread out as there is no pedestrian in front of them, which leads to a decrease in the pedestrian density.

With the exact solution known, the mean and deviation of the density ρ at position x and time t can be derived from $\mathbb{E}[\rho(x,t,\xi)] = \int_\Theta \rho(x,t,\xi) w(\xi) d\xi$ and $\mathbb{D}[\rho(x,t,\xi)] = \mathbb{E}[\rho^2(x,t,\xi)] - \mathbb{E}[\rho(x,t,\xi)]^2$. For the first example, the uniformly distributed random variable $\xi \sim \mathcal{U}(0, \rho_{\max}/2)$ yields a PDF $w(\xi) = 2/\rho_{\max}$. Through simple calculations, the following results are obtained for $0 \le \gamma \le 1$:

$$\mathbb{E}[\rho(x,t,\xi)] = \frac{\rho_{\max}}{4}(1-\gamma^2), \quad \mathbb{D}[\rho(x,t,\xi)] = \frac{\rho_{\max}^2}{48}(1-\gamma)^3(1+3\gamma).$$

The mean and deviation of the random variable ξ are $\mathbb{E}[\xi] = \rho_{\max}/4$ and $\mathbb{D}[\xi] = \rho_{\max}^2/48$, respectively. The relations between the statistical properties of the solution $\rho(\cdot,\xi)$ and the random input ξ are written as

$$\mathbb{E}[\rho(\cdot,\xi)] = \mathbb{E}[\xi](1-\gamma^2), \quad \mathbb{D}[\rho(\cdot,\xi)] = \mathbb{D}[\xi](1-\gamma)^3(1+3\gamma), \quad 0 \le \gamma \le 1. \tag{10}$$

Here, $\gamma = \frac{x}{u_f t}$ actually represents the relative position of a pedestrian within the advancing crowd, where $\gamma = 0$ and $\gamma = 1$ signify the tail and head of the crowd, respectively. $\mathcal{R}_{\mathbb{E}}(\cdot) = \mathbb{E}[\rho(\cdot,\xi)]/\mathbb{E}[\xi]$ is defined as the ratio between the mean of ρ and ξ, while $\mathcal{R}_{\mathbb{D}}(\cdot) = \mathbb{D}[\rho(\cdot,\xi)]/\mathbb{D}[\xi]$ denotes the ratio between the deviation of ρ and ξ. $\mathcal{R}_{\mathbb{E}}$ and $\mathcal{R}_{\mathbb{D}}$ quantify the responses of pedestrian density to random inputs at different locations and times. From (10), these ratios can be directly derived as $\mathcal{R}_{\mathbb{E}}(\gamma) = 1-\gamma^2$ and $\mathcal{R}_{\mathbb{D}}(\gamma) = (1-\gamma)^3(1+3\gamma)$ for $0 \le \gamma \le 1$. Fig. 2(a) plots the graphs of $\mathcal{R}_{\mathbb{E}}$ and $\mathcal{R}_{\mathbb{D}}$, which demonstrate that both ratios decrease as γ increases from 0 to 1. $\mathcal{R}_{\mathbb{E}}$ falls because the pedestrian density decreases from the tail of the crowd to the head, while the fall in $\mathcal{R}_{\mathbb{D}}$ is due to the crowd spreading out. This is consistent with real-world observations because the spreading out of a crowd to low-density regions reduces the number of pedestrians per unit length and the diversity of the system.

For the second example, if the random variable is assumed to be uniformly distributed, i.e., $\xi \sim \mathcal{U}(0, \rho_{\max})$, then the exact solution (Fig. 1(b)) is a shockwave when $t < L/u_f$:

$$\rho(x,t,\xi) = \begin{cases} \xi, & x < L - \frac{\xi}{\rho_{\max}} u_f t, \\ \rho_{\max}, & L - \frac{\xi}{\rho_{\max}} u_f t < x < L, \end{cases}$$

where the traveling speed $-\frac{\xi}{\rho_{\max}} u_f$ is derived based on the Rankine–Hugoniot jump condition $s = \frac{f(\xi) - f(\rho_{\max})}{\xi - \rho_{\max}}$ (LeVeque, 1992). By defining $\gamma = \frac{L-x}{u_f t} > 0$, the solution can be expressed as

$$\rho(x,t,\xi) = \begin{cases} \rho_{\max}, & 0 < \gamma < \frac{\xi}{\rho_{\max}}, \\ \xi, & \gamma > \frac{\xi}{\rho_{\max}}. \end{cases} \tag{11}$$

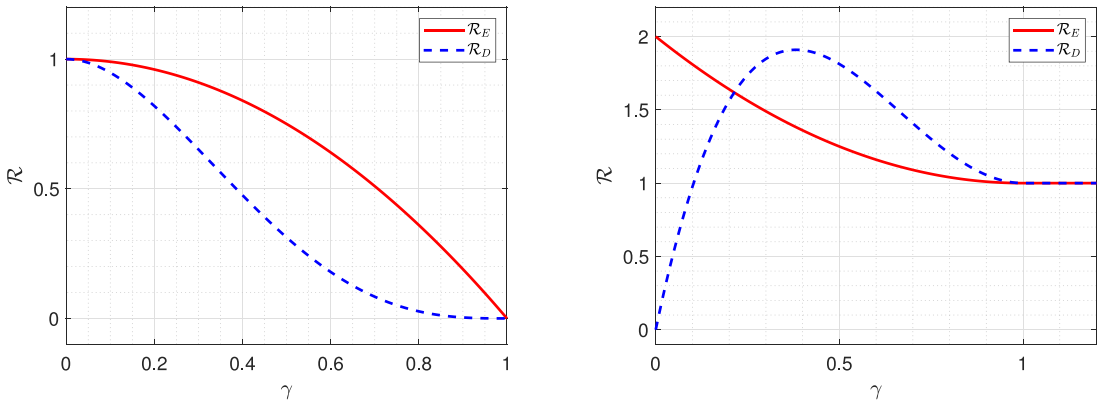

(a) Example 1 with $\gamma = \frac{x}{u_f t}$. (b) Example 2 with $\gamma = \frac{L-x}{u_f t}$.

Fig. 2. The graphs of $\mathcal{R}_{\mathbb{E}}$ and $\mathcal{R}_{\mathbb{D}}$ in terms of γ. Left: result of example 1 with $\gamma = \frac{x}{u_f t}$. Right: result of example 2 with $\gamma = \frac{L-x}{u_f t}$.

Here, the interval $(0, \frac{\xi}{\rho_{\max}})$ corresponds to the region where the pedestrians have met a jam, decelerated to a stop, and formed a congested crowd. Conversely, the interval $(\frac{\xi}{\rho_{\max}}, +\infty)$ represents the region where the pedestrians have not been affected by the jam in front of them. Similarly, the mean and deviation of the density can be calculated as

$$0 < \gamma < 1: \quad \mathbb{E}[\rho(x,t,\xi)] = \frac{\rho_{\max}}{2}\left[1 + (\gamma-1)^2\right], \quad \mathbb{D}[\rho(x,t,\xi)] = \frac{\rho_{\max}^2}{12}\gamma(12 - 24\gamma + 16\gamma^2 - 3\gamma^3),$$

$$\gamma > 1: \quad \mathbb{E}[\rho(x,t,\xi)] = \frac{\rho_{\max}}{2}, \quad \mathbb{D}[\rho(x,t,\xi)] = \frac{\rho_{\max}^2}{12}.$$

As $\mathbb{E}[\xi] = \rho_{\max}/2$ and $\mathbb{D}[\xi] = \rho_{\max}^2/12$, the ratio functions are

$$\mathcal{R}_{\mathbb{E}}(\gamma) = \begin{cases} 1 + (\gamma-1)^2, & 0 < \gamma < 1, \\ 1, & \gamma > 1, \end{cases} \quad \mathcal{R}_{\mathbb{D}}(\gamma) = \begin{cases} \gamma(12 - 24\gamma + 16\gamma^2 - 3\gamma^3), & 0 < \gamma < 1, \\ 1, & \gamma > 1. \end{cases}$$

The parameter $\gamma = \frac{L-x}{u_f t}$ represents the distance from a pedestrian's position to the initial jam location. Fig. 2(b) plots the graphs of $\mathcal{R}_{\mathbb{E}}$ and $\mathcal{R}_{\mathbb{D}}$. $\mathcal{R}_{\mathbb{E}}$ is observed to be larger in the region where the shock is generated and congestion occurs ($0 < \gamma < 1$) than in the region not influenced by the shock ($\gamma > 1$). Moreover, $\mathcal{R}_{\mathbb{E}}$ decreases as γ increases, because the response of pedestrians to the randomness is attenuated at locations distant from the jam. $\mathcal{R}_{\mathbb{D}}$, by comparison, exhibits a slight variation within the region $(0, 1)$. When γ is close to 0, $\mathcal{R}_{\mathbb{D}}$ tends to 0. This is because pedestrians always stop at this location when they encounter congestion, and the density attains its highest density ($\rho_{\max}$). Because the position of the shock is uncertain, $\mathcal{R}_{\mathbb{D}}$ begins to increase and reaches its maximum value when $\gamma \approx \frac{1}{3}$. This maximum exceeds the constant value $\mathcal{R}_{\mathbb{D}} = 1$ in the region $(1, +\infty)$, which indicates that the congestion and shock generation would inject more variations and risk into the system. Thereafter, $\mathcal{R}_{\mathbb{D}}$ begins to decrease, similar to $\mathcal{R}_{\mathbb{E}}$. However, compared with that in the first example, the decline in $\mathcal{R}_{\mathbb{D}}$ due to congestion is delayed. Therefore, considerable time is required to eliminate the effects of the high variance caused by congestion.

The analytical analysis of these two examples illustrates that crowd evacuation can effectively reduce the variation and risk created by randomness, whereas congestion can significantly increase the uncertainty within the system. Furthermore, in terms of the pedestrian density, the decrease in deviation within the system tends to lag behind the decrease in mean. Similar observations are also reported in the numerical results. The analytical examination using the continuum model provides valuable insights into the properties of pedestrian flow propagation in a stochastic environment.

For a general model (2), for which the exact solution and statistics are not explicitly known, the ME-PCM presented next constitutes a rapid method to numerically derive the solution and its statistical properties.

2.3. Multi-element probabilistic collocation method

This part introduces the details of ME-PCM application to the generalized pedestrian flow model as described before, including the decomposition of random space, sampling and reconstruction. The strategy transforms the original problem into a collection of deterministic samples, to which the well-established solution algorithm for deterministic PDEs can be applied. The overall procedure of the ME-PCM is finally summarized to facilitate the application of this methodology by interested researchers.

The target solution $\boldsymbol{U}(\boldsymbol{x}, t, \xi)$ of system (2) is assumed to be a second-order space–time-related random field. In contrast to MC methods, gPC type methods adopt a functional expression of the stochastic process:

$$\boldsymbol{U}(\boldsymbol{x}, t, \xi) = \sum_{j=0}^{+\infty} \hat{\boldsymbol{U}}_j(\boldsymbol{x}, t)\boldsymbol{\Phi}_j(\xi), \tag{12}$$

where Φ_j is the orthogonal polynomial basis, and $\hat{U}_j$ denotes the corresponding coefficients. This expression was first proposed by Wiener (1938), using Hermite polynomials to represent Gaussian stochastic processes. According to the theorem presented by Cameron and Martin (1947), the polynomial chaos expansion converges for a second-order process in the L_2 sense. Therefore, a truncated expansion with N_p+1 terms $\sum_{j=0}^{N_p}\hat{U}_j(x,t)\Phi_j(\xi)$ provides an appropriate approximation. As described before, for a highly-nonlinear model, the solution involves a discontinuity or sharp region in the random space, leading to poor convergence when using high-degree global polynomials. In addition, the gPC method may not be suitable for certain long-term problems (Gerritsma et al., 2010). The statistical properties of the solution change over time, and the orthogonal polynomial basis that leads to exponential convergence in the initial period may not be effective in later stages.

To address this problem, a multi-element probabilistic collocation method is considered here (Wan and Karniadakis, 2005, 2006; Foo et al., 2008). The main concept of the ME-PCM is to decompose the random space into elements and represent the solution using element-wise polynomials. In this framework, the ME-PCM yields more accurate approximations of the solution distribution with a minimal increase in the computational cost. The procedure involves three key steps, namely decomposing the random space, sampling, and reconstructing expansion coefficients. The spatial and temporal discretization schemes are not limited and are discussed later.

Decomposition is achieved by discretizing the random space Θ into N_e nonoverlapping meshes of open intervals:

$$\begin{cases} B_k = (a_k, b_k), \\ \Theta = \cup_{k=1}^{N_e} B_k, \\ B_{k_1} \cap B_{k_2} = \varnothing, \quad \forall\ k_1 \neq k_2, \end{cases} \tag{13}$$

where $k, k_1, k_2 = 1, \dots, N_e$. Here, a_k and b_k are finite or infinite in $\mathbb{R}$, allowing the decomposition to be applied to any type of continuous distribution.

Definition 1. Based on the decomposition, for each random element, the indicator random variable is defined as

$$I_{B_k} = \begin{cases} 1, & \text{if} \quad \xi \in B_k, \\ 0, & \text{otherwise.} \end{cases} \qquad k = 1, 2, \dots, N_e. \tag{14}$$

This leads to a decomposition of the sample space $\Omega = \cup_{k=1}^{N_e} I_{B_k}^{-1}(1)$, where $I_{B_{k_1}}^{-1}(1) \cap I_{B_{k_2}}^{-1}(1) = \varnothing, \forall k_1 \neq k_2$.

Definition 2. In each element B_k, a new local random variable

$$\xi_k(\omega) : I_{B_k}^{-1}(1) \mapsto B_k \tag{15}$$

is defined in the probability space $(I_{B_k}^{-1}(1), \mathcal{F} \cap I_{B_k}^{-1}(1), P(\cdot | I_{B_k} = 1))$ with a conditional PDF

$$\hat{w}_k(\xi_k | I_{B_k} = 1) = \frac{w(\xi_k)}{\int_{B_k} w(\xi) \mathrm{d}\xi}, \tag{16}$$

where $\int_{B_k} w(\xi) d\xi > 0$.

To this end, the random space Θ is decomposed and local random variables ξ_k are obtained. Regarding the conditional PDF $\hat{w}_k$ as a weight function, a local orthogonal polynomial basis $\left\{\Phi_{k,j}(\xi_k)\right\}_{j=0}^{N_p}$ is constructed by adopting the following Stieltjes procedure (Gautschi, 1982), where N_p+1 is the number of orthogonal basis functions.

Theorem 1 (*Stieltjes Procedure*). *The basis functions satisfy a three-term recurrence relation*

$$\begin{aligned} &\Phi_{k,j+1}(\xi_k) = (\xi_k - a_{k,j})\Phi_{k,j}(\xi_k) - b_{k,j}\Phi_{k,j-1}(\xi_k), \quad j = 0, 1, \dots, \\ &\Phi_{k,0}(\xi_k) = 1, \quad \Phi_{k,-1}(\xi_k) = 0. \end{aligned} \tag{17}$$

where the recurrence coefficients $a_{k,j}, b_{k,j}$ *are*

$$a_{k,j} = \frac{\mathbb{E}[\xi_k \Phi_{k,j}^2]}{\mathbb{E}[\Phi_{k,j}^2]}, \quad j = 0, 1, 2, \dots, \tag{18}$$

$$b_{k,0} = \mathbb{E}[\Phi_{k,0}^2], \quad b_{k,j} = \frac{\mathbb{E}[\Phi_{k,j}^2]}{\mathbb{E}[\Phi_{k,j-1}^2]}, \quad j = 1, 2, \dots. \tag{19}$$

In element B_k, the polynomial basis functions are orthogonal with respect to $\hat{w}_k$:

$$\mathbb{E}[\Phi_{k,i}\Phi_{k,j}] = \int_{B_k} \Phi_{k,i}(\xi_k)\Phi_{k,j}(\xi_k)\hat{w}_k(\xi_k | I_{B_k} = 1)\mathrm{d}\xi_k = 0, \quad \forall\ i \neq j. \tag{20}$$

The local approximation of $\boldsymbol{U}(\boldsymbol{x}, t, \xi)$ in element B_k is efficiently expressed as (Wan and Karniadakis, 2006)

$$\boldsymbol{U}(\boldsymbol{x}, t, \xi_k)|_{\xi_k \in B_k} \approx \hat{\boldsymbol{U}}_k(\boldsymbol{x}, t, \xi_k) = \sum_{j=0}^{N_p} \hat{\boldsymbol{U}}_{k,j}(\boldsymbol{x}, t)\Phi_{k,j}(\xi_k). \tag{21}$$

Consequently, the approximation on the entire random field is expressed as

$$\boldsymbol{U}(\boldsymbol{x},t,\xi)|_{\xi\in\Theta}=\sum_{k=1}^{N_e}\hat{\boldsymbol{U}}_k(\boldsymbol{x},t,\xi)I_{B_k}=\sum_{k=1}^{N_e}\sum_{j=0}^{N_p}\hat{\boldsymbol{U}}_{k,j}(\boldsymbol{x},t)\boldsymbol{\Phi}_{k,j}(\xi)I_{B_k}. \tag{22}$$

The next step is to determine the coefficients $\hat{\boldsymbol{U}}_{k,j}$. Unlike the SG method, which requires solving a new group of equations with respect to coefficients in the expansion, the ME-PCM derives the coefficients based on sampling. The ME-PCM is one example of a stochastic collocation (SC) method (Xiu, 2009), a category of methods that have emerged as promising computational tools for uncertainty quantification owing to their robustness and unlimited numerical schemes. Leveraging a suitable quadrature rule, the SC scheme can be considered as an approximation of the SG scheme (Zhong and Shu, 2022). In each element B_k, the Galerkin projection onto the space spanned by orthogonal polynomials is the best approximation in the L_2 sense (Kincaid and Cheney, 2009). The coefficient takes the form

$$\hat{\boldsymbol{U}}_{k,j}(\boldsymbol{x},t)=\frac{1}{\mathbb{E}[\boldsymbol{\Phi}_{k,j}^2]}\int_{B_k}\boldsymbol{U}(\boldsymbol{x},t,\xi_k)\boldsymbol{\Phi}_{k,j}(\xi_k)\hat{w}_k(\xi_k|I_{B_k}=1)\mathrm{d}\xi_k. \tag{23}$$

In the pseudo-projection SC approach (Foo et al., 2008; Xiu, 2009), a Gauss quadrature rule is applied to approximate the integration in (23). Specifically,

$$\hat{\boldsymbol{U}}_{k,j}(\boldsymbol{x},t)\approx\frac{1}{\mathbb{E}[\boldsymbol{\Phi}_{k,j}^2]}\sum_{s=1}^{N_s}\alpha_k^s\boldsymbol{U}(\boldsymbol{x},t,\xi_k^s)\boldsymbol{\Phi}_{k,j}(\xi_k^s), \tag{24}$$

where $\{\xi_k^s\}_{s=1}^{N_s}$ represents the integration points of the quadrature rule on B_k with weights $\{\alpha_k^s\}_{s=1}^{N_s}$. The equation sets (2) are then enforced at node ξ_k^s for all $k=1,\dots,N_e, s=1,\dots,N_s$:

$$\partial_t\boldsymbol{U}(\boldsymbol{x},t,\xi_k^s)+\mathcal{L}(\boldsymbol{U}(\boldsymbol{x},t,\xi_k^s))=0, \qquad \forall(\boldsymbol{x},t)\in D\times(0,T], \tag{25a}$$

$$\boldsymbol{U}(\boldsymbol{x},0,\xi_k^s)=\boldsymbol{U}^0(\boldsymbol{x},\xi_k^s), \qquad \forall\boldsymbol{x}\in D, \tag{25b}$$

$$\boldsymbol{U}(\boldsymbol{x},t,\xi_k^s)=\boldsymbol{G}(t,\xi_k^s), \qquad \forall(\boldsymbol{x},t)\in\partial D\times(0,T]. \tag{25c}$$

For each fixed ξ_k^s, (25a) with (25b) and (25c) represent a deterministic system, which can be solved using a well-established algorithm. The algorithm for the deterministic problem has no limitations and can be viewed as a black box in the ME-PCM procedure. This ease of implementation is an important advantage of sampling-based methods, including MC methods. After repeatedly running the code at different input parameter values, the solution ensemble $\cup_{k=1}^{N_e}\cup_{s=1}^{N_s}\{\boldsymbol{U}(\boldsymbol{x},t,\xi_k^s)\}$ is derived, and then in each random space B_k, the expansion is reconstructed using (21) and (24).

From the gPC expansion (21) in element B_k and orthogonality of the basis, the local mean and deviation are directly obtained as

$$\mathbb{E}[\boldsymbol{U}(\cdot,\xi_k)]=\hat{\boldsymbol{U}}_{k,0},\quad \mathbb{D}[\boldsymbol{U}(\cdot,\xi_k)]=\sum_{j=1}^{N_p}\hat{\boldsymbol{U}}_{k,j}^2\mathbb{E}[\boldsymbol{\Phi}_{k,j}^2],\quad \text{in element } B_k. \tag{26}$$

Here, "·" represents spatial and time coordinates. The global mean and deviation are simply derived as

$$\mathbb{E}[\boldsymbol{U}(\cdot,\xi)]=\sum_{k=1}^{N_e}\hat{\boldsymbol{U}}_{k,0}\int_{B_k}w(\xi)d\xi, \tag{27}$$

$$\mathbb{D}[\boldsymbol{U}(\cdot,\xi)]=\sum_{k=1}^{N_e}\left[\sum_{j=1}^{N_p}\hat{\boldsymbol{U}}_{k,j}^2\mathbb{E}[\boldsymbol{\Phi}_{k,j}^2]+\left(\hat{\boldsymbol{U}}_{k,0}-\mathbb{E}[\boldsymbol{U}(\cdot,\xi)]\right)^2\right]\int_{B_k}w(\xi)d\xi. \tag{28}$$

Moreover, the 95% confidence interval at a space–time point is defined as $[\boldsymbol{S}_a(\cdot),\boldsymbol{S}_b(\cdot)]$, satisfying $P\left(\boldsymbol{S}_a(\cdot)<\boldsymbol{U}(\cdot,\xi)<\boldsymbol{S}_b(\cdot)\right)=0.95$. $\boldsymbol{S}_a$ and $\boldsymbol{S}_b$ are respectively the minimum and maximum of the 95% confidence interval. The above statistical information can be quickly computed using the functional expression (22) for $\boldsymbol{U}$.

The accuracy of the ME-PCM depends on the number of random elements N_e and the polynomial order N_p. It has been proven (Foo et al., 2008) that for a fixed N_p, the ME-PCM solution has a moments error of $O(N_e^{-2(N_p+1)})$ for a smooth function, neglecting the error in spatial and temporal discretization. The number of integration points, N_s, must match N_e to ensure accuracy. In this study, N_s is set as N_p+1 to ensure that the approximation (24) is exactly satisfied when the true solution is a polynomial of order N_p. The total number of sample points is $N=N_e\cdot N_s=N_e(N_p+1)$, and the moments error can be expressed as $O(N^{-2(N_p+1)})$ for fixed N_p. For smooth functions, the ME-PCM solution has a convergence rate of $O(N^{-4})$ when $N_p=1$, which is much better than the half-order convergence $O(N^{-1/2})$ of the MC method. In terms of the non-linear pedestrian flow models considered here, although the expected convergence may not be realized without a guarantee of solution regularity, this study still obtains results having an improved convergence rate compared with the results of MC methods. This is discussed in detail in the numerical results section.

The desired accuracy can be maintained using two strategies, namely refining the decomposition (increasing N_e) and increasing the polynomial order (increasing N_p). Adaptive refinement (Wan and Karniadakis, 2005) can be introduced to accelerate convergence. In maintaining algorithm efficiency, uniform decomposition can be first considered, and the "off-line" element-wise

polynomial basis needs to be constructed only once. In practice, the random variable ξ_k in element B_k can be linearly transformed according to

$$\xi_k = \frac{b_k - a_k}{2}\eta_k + \frac{b_k + a_k}{2} \tag{29}$$

into a random variable η_k defined on $[-1, 1]$. The PDF of η_k is defined as

$$i\bar{w}_k(\eta_k | I_{B_k} = 1) = \frac{\partial \xi_k}{\partial \eta_k} i\hat{w}_k(\xi_k | I_{B_k} = 1) = \frac{b_k - a_k}{2} \frac{w(\xi_k(\eta_k))}{\int_{B_k} w(\xi) d\xi}. \tag{30}$$

The ME-PCM is then introduced with respect to η_k adopting a standard procedure in the unit interval $[-1, 1]$. For the element B_k having an infinite boundary, the probability $\int_{B_k} w(\xi) d\xi$ on B_k is always small. As the values in these elements typically have no practical meaning, they can be eliminated at the cost of negligible error.

The following algorithm 1 outlines the overall algorithm flow. We assume an explicit temporal discretization scheme is used to update (25a) in the time sequence $t_0, t_1, \dots, t_n$.

Algorithm 1 ME-PCM procedure

1: **Step 1**: Discretize the random space Θ and spatial space D. In each element B_k, construct local polynomial basis $\left\{\Phi_{k,j}\right\}_{j=0}^{N_p}$ with respect to the corresponding conditional PDF $i\hat{w}_k$, and derive integration points and weights $\left\{(\xi_k^s, \alpha_k^s)\right\}_{s=1}^{N_s}$. Initialize the solution $\boldsymbol{U}(\boldsymbol{x}, t_0, \xi)$.
2: **Step 2:** Loop for each time step $t_n (n \geq 0)$:
3: Determine the solution $\boldsymbol{U}(\boldsymbol{x}, t_n, \xi_k^s)$;
4: Loop for each sample point ξ_k^s:
5: Solve (25) using existing numerical solvers.
6: Derive the solution ensemble $\cup_{k=1}^{N_e} \cup_{s=1}^{N_s} \left\{\boldsymbol{U}(\boldsymbol{x}, t_{n+1}, \xi_k^s)\right\}$;
7: Reconstruct the solution $\boldsymbol{U}(\boldsymbol{x}, t_{n+1}, \xi)$;
8: **Step 3**: Output the deserved statistical information.

The complexity of the ME-PCM algorithm mainly depends on the number of samples $N = N_e(N_p + 1)$, as the cost associated with the construction of orthogonal polynomials is negligible. Note that for every random input ξ_k^s, the simulations are independent at each time step. Parallelization can thus be applied to further reduce the computational cost.

3. Numerical example

To demonstrate the effectiveness of the ME-PCM, this section uses the well-known Hughes model by appending a random variable to the boundary condition. A two-dimensional numerical example that includes a corridor with an obstacle is presented, and the inflow demand at the entrance is assumed to follow a lognormal distribution. High-order finite difference schemes are applied to solve deterministic PDEs as samples. Statistical information, including the expectation, standard deviation, and confidence interval, is efficiently derived to quantify the locations where exceptional congestion varies from the average level in the walking facility. Simulations are performed using different numbers of random elements and polynomial basis functions to test the converge performance of the ME-PCM. The numerical results show that the ME-PCM accelerates simulations relative to MC methods, even in scenarios with increased variance.

3.1. Hughes model with randomized inflow demand

A railway platform including a corridor with an obstacle, as illustrated in Fig. 3, is considered. Pedestrians enter from the left entrance and leave through the right exit. The boundary $\partial D = \Gamma_o \cup \Gamma_d \cup \Gamma_h$, where Γ_o, Γ_d, and Γ_h denote the entrance, exit, and wall of the walking facility, respectively. Hughes model (Hughes, 2002) is considered to describe pedestrian crowd dynamics in which pedestrians move along the path that minimizes their travel time while avoiding extremely high densities. The model is given by

$$\rho_t + \nabla \cdot \left(-\rho \frac{u(\rho)}{c(\rho)} \nabla \phi\right) = 0, \qquad \forall (\boldsymbol{x}, t, \xi) \in D \times (0, T] \times \Theta, \tag{31a}$$

$$|\nabla \phi| = c(\rho), \qquad \forall (\boldsymbol{x}, t, \xi) \in D \times (0, T] \times \Theta. \tag{31b}$$

The function $\rho(\boldsymbol{x}, t, \xi)$ represents the time-varying pedestrian density, and $\phi(\boldsymbol{x}, t, \xi)$ represents the walking time potential along the instantaneous shortest path from location $\boldsymbol{x}$ to the destination $\Gamma_d (\phi = 0)$, based on the traffic condition at moment t. $\boldsymbol{f} = -\rho u(\rho)/c(\rho) \nabla \phi$ is the flow vector. $u(\rho)$ is the local walking speed and can be determined using various types of pedestrian fundamental diagrams, such as Greenshields's model (Huang et al., 2009a), Drake's model (Wong et al., 2010), and Newell's model (Newell, 1961). In this study, Newell's model is applied because of its flexibility in fitting observed speed–density diagrams (Parisi et al., 2021). The model is given by

$$u(\rho) = u_f \left\{1 - \exp\left[\frac{c_0}{u_f}\left(1 - \frac{\rho_{\max}}{\rho}\right)\right]\right\}, \tag{32}$$

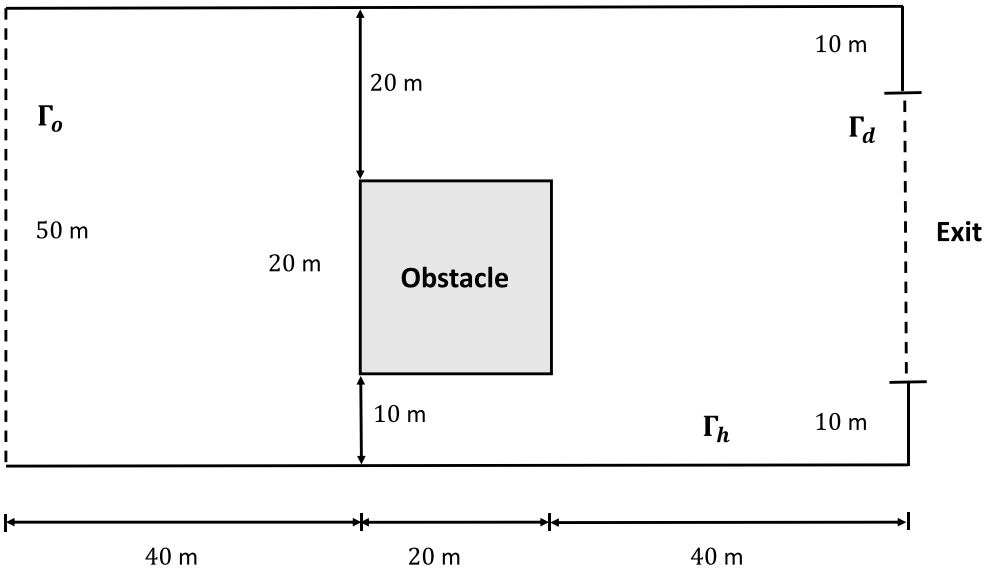

Fig. 3. The geometry of the railway platform.

where u_f is the average walking speed of pedestrians, and c_0 is a parameter governing the backward wave speed at maximum density, $\rho_{\max}$. The cost function $c(\rho)$ is defined as $c(\rho) = 1/u(\rho) + g(\rho)$, where $1/u(\rho)$ represents the local cost associated with the (estimated) travel time, and $g(\rho)$ represents the level of discomfort assumed to monotonically increase with density. Eq. (31a) is the continuity equation and Eq. (31b) is an eikonal equation, which ensures that pedestrians select routes that minimize their individual travel cost to the destination, considering the instantaneous travel cost information.

Randomness enters the system from the following initial boundary conditions:

$$\boldsymbol{f}(\boldsymbol{x},t,\xi)\cdot\boldsymbol{n}(\boldsymbol{x}) = \xi q(\boldsymbol{x},t), \qquad \forall(\boldsymbol{x},t,\xi)\in\Gamma_o\times(0,T]\times\Theta, \tag{33a}$$

$$\rho(\boldsymbol{x},0,\xi) = \rho^0(\boldsymbol{x}), \qquad \forall(\boldsymbol{x},\xi)\in D\times\Theta, \tag{33b}$$

$$\phi(\boldsymbol{x},t,\xi) = 0, \qquad \forall(\boldsymbol{x},t,\xi)\in\Gamma_d\times(0,T]\times\Theta. \tag{33c}$$

Here, $\boldsymbol{n}(\boldsymbol{x})$ is a unit outer normal vector that points outward from the domain boundary, and $\rho^0(\boldsymbol{x})$ is the initial pedestrian density. $q(\boldsymbol{x},t)$ represents the number of pedestrians crossing a unit width of the original segment and is given as a deterministic time-varying demand function. ξ is a random variable satisfying the following assumptions of demand stochasticity.

1. Stochasticity arises from factors influencing the traffic demand q at the entrance. The impact of these factors is reflected in the average traffic demand q being scaled up or down by the parameter ξ.
2. The scaling parameter ξ is treated as a random input following a lognormal distribution.

For instance, on a rainy day, a greater number of people are observed to enter underground stations, increasing the traffic demand ($\xi > 1$) at the entrance (although the demand may vary with time). The scaling parameter ξ remains fixed during the brief period in which people enter and exit the platform, as weather conditions typically do not change appreciably within a few minutes. On a sunny day, ξ is smaller ($\xi < 1$) but remains fixed in a given period. Under random conditions, the pedestrian density varies within a range, and this variation cannot be captured by a deterministic model within average demand. The random variable ξ scaling the averaged traffic demand $q(\boldsymbol{x},t)$ is independent of location and time, indicating that for each random event, the demand is entirely scaled by the same parameter. This configuration is consistent with the definition of day-to-day demand stochasticity, where differences occur on different days rather than on the same day. Notably, to validate the effectiveness of the ME-PCM, the model used here is the same as Hughes model, except that the boundary condition is assumed to be randomized. The ME-PCM can also be implemented for other similar models with random inputs.

3.2. Numerical schemes for solving deterministic PDEs

There has been abundant research on numerical schemes for solving Hughes model, such as the finite difference (Huang et al., 2009a), finite volume, and finite element schemes (Jiang et al., 2011; Twarogowska et al., 2014; Ghattassi and Masmoudi, 2023). Based on finite difference schemes, Huang et al. (2009a) proposed an efficient algorithm for the deterministic problem. This study adopts their algorithm for its ability to capture shock propagation accurately in pedestrian crowd dynamics. A brief review is presented here.

The physical domain is divided by fixed Cartesian meshes:

$$x_{i+1} = x_i + \Delta x, \quad y_{j+1} = y_j + \Delta y, \tag{34}$$

where Δx and Δy are uniform mesh sizes in the x- and y-directions, respectively. $\rho_{i,j}$ and $\boldsymbol{f}_{i,j} = ((f_1)_{i,j}, (f_2)_{i,j})$ denote the approximations of ρ and $\boldsymbol{f}$, respectively, at grid point (x_i, y_j). The semi-discrete form of Eq. (31a) is

$$\frac{d}{dt}\rho_{i,j} = -\frac{1}{\Delta x}\left((\hat{f}_1)_{i+1/2,j} - (\hat{f}_1)_{i-1/2,j}\right) - \frac{1}{\Delta y}\left((\hat{f}_2)_{i,j+1/2} - (\hat{f}_2)_{i,j-1/2}\right). \tag{35}$$

The numerical fluxes $(\hat{f}_1)_{i+1/2,j}$ and $(\hat{f}_2)_{i,j+1/2}$ at the half-point are obtained by the one-dimensional fifth order weighted essentially non-oscillatory (WENO) finite difference scheme based on Lax–Friedrichs flux splitting (Jiang and Shu, 1996). After spatial discretization, the semi-discrete scheme is equivalent to a first-order ordinary differential equation system $\rho_t = L(\rho)$, where $L(\rho)$ is the spatial operator. Subsequently, the third-order total variation diminishing Runge–Kutta time integration (Shu and Osher, 1988), which is a convex combination of three Euler forward steps, is applied to ensure system evolution:

$$\rho^{(1)} = \rho^n + \Delta t L(\rho^n), \tag{36a}$$

$$\rho^{(2)} = \frac{3}{4}\rho^n + \frac{1}{4}\left(\rho^{(1)} + \Delta t L(\rho^{(1)})\right), \tag{36b}$$

$$\rho^{n+1} = \frac{1}{3}\rho^n + \frac{2}{3}\left(\rho^{(2)} + \Delta t L(\rho^{(2)})\right), \tag{36c}$$

where Δt is the time step and the superscript denotes the time level. The discretized form of the eikonal equation (31b) is

$$\hat{H}\left((\phi_x)^-_{i,j}, (\phi_x)^+_{i,j}; (\phi_y)^-_{i,j}, (\phi_y)^+_{i,j}\right) = C(\rho(x_i, y_j, t^n)), \tag{37}$$

where $\hat{H}$ is the Godunov-type monotone Hamiltonian, and $(\phi_x)^{\pm}$ and $(\phi_y)^{\pm}$ are WENO approximations of the left and right derivatives of ϕ in the x and y directions, respectively. The fast-sweeping method with the third-order WENO scheme (Zhang et al., 2006) is applied to solve this equation.

3.3. Example settings

As shown in Fig. 3, a railway platform has a length of 100 m and width of 50 m. The obstacle placed in the middle of the platform has a size of 20 m by 20 m. The time horizon T is 240 s. The discomfort function is set as $g(\rho) = 0.002\rho^2$. The maximum density $\rho_{\max}$ and parameter c_0 in Eq. (32) are set as 6 ped/m^2 and 0.4, respectively. The average time-varying demand function is expressed as

$$q(0, y, t) = \begin{cases} t/100 & 0 \le t < 60, \\ 1.2 - t/100 & 60 \le t < 120, \\ 0 & 120 \le t, \end{cases} \tag{38}$$

with the unit being ped/m/s. The random input ξ follows a lognormal distribution in two cases:

- $\xi \sim \text{Lognormal}(1.0, 0.1^2)$, MEAN = 1.0, SDEV = 0.1;
- $\xi \sim \text{Lognormal}(1.0, 0.2^2)$, MEAN = 1.0, SDEV = 0.2.

The rectangular domain $[0, 100] \times [0, 50]$ (units: m) is discretized into 100×50 uniformly spaced grid points for the numerical simulation. This problem, formulated as a set of PDEs with initial and boundary conditions, is solved using the efficient numerical schemes described earlier. To ensure numerical stability, the time step is restricted as $\Delta t = \text{CFL}/\left(\frac{\alpha}{\Delta x} + \frac{\beta}{\Delta y}\right)$, where the coefficient CFL = 0.5, $\alpha = \max_{i,j} |u_1|, \beta = \max_{i,j} |u_2|$, and (u_1, u_2) is the velocity vector.

To investigate the convergence rate of the ME-PCM, the global relative root mean square error (RRMSE) is considered:

$$E_\rho = \frac{\sqrt{\frac{1}{N_g}\sum_{i,j,k}(\rho^{(\text{ref})}_{i,j,k} - \rho^{(N_e,N_p)}_{i,j,k})^2}}{\frac{1}{N_g}\sum_{i,j,k}\rho^{(\text{ref})}_{i,j,k}} \times 100\%, \tag{39a}$$

$$E_\sigma = \frac{\sqrt{\frac{1}{N_g}\sum_{i,j,k}(\sigma^{(\text{ref})}_{i,j,k} - \sigma^{(N_e,N_p)}_{i,j,k})^2}}{\frac{1}{N_g}\sum_{i,j,k}\sigma^{(\text{ref})}_{i,j,k}} \times 100\%, \tag{39b}$$

where the subscript k represents the integer time points satisfying $t_k = k, k = 1, 2, \ldots, 240$. E_ρ and E_σ denote the RRMSEs of the mean (MEAN) and standard deviation (SDEV) of the density, respectively. $\rho^{(N_e,N_p)}_{i,j,k}$ and $\sigma^{(N_e,N_p)}_{i,j,k}$ denote the MEAN and SDEV of the density for the grid point (x_i, y_j, t_k) in a case involving N_e random elements and N_p polynomial basis functions, respectively. $\rho^{(\text{ref})}_{i,j,k}$ and $\sigma^{(\text{ref})}_{i,j,k}$ are the reference solutions obtained from the ME-PCM results for a sufficiently large number of sample points. Here, ME-PCM solutions with $N_e = 256, N_p = 5$ are regarded as the benchmark solution for comparative analyses. N_g is the total number of space–time grid points. The total MEAN and SDEV of the density over the entire spatial space at time t_k are defined as

$$\text{Total}_\rho(t_k) = \sum_{i,j} \rho^{(Ne,Np)}_{i,j,k}, \tag{40a}$$

$$\text{Total}_{\sigma}(t_k) = \sum_{i,j} \sigma_{i,j,k}^{(Ne,Np)}, \tag{40b}$$

which illustrate the variations in the statistics over time. To quantify the locations in walking facilities where the average pedestrian density is moderate but exceptional congestion can occur with a large variance, this study defines these risk regions as

$$\Omega_r(t) = \left\{(x,y) \in D | S_b(x,y,t) > C_r \cdot \mathbb{E}[\rho(x,y,t,\xi)]\right\}, \tag{41}$$

where $\mathbb{E}[\rho(\cdot,\xi)]$ is the mean, and $S_b(\cdot)$ is the maximum of the 95% confidence interval $\left[S_a(\cdot), S_b(\cdot)\right]$ of the pedestrian density distribution. The constant C_r is taken as 2.0 in this example to represent the locations Ω_r where the maximum of the pedestrian density distribution in the 95% confidence interval is twice the average level under the random demand.

3.4. Numerical results

3.4.1. Case 1: $\xi \sim Lognormal(1.0, 0.1^2)$

The lognormal variable $\xi \sim \text{Lognormal}(1.0, 0.1^2)$ is first tested using the ME-PCM. $N_e = 20$ random elements and $N_p = 3$ polynomial bases are used to derive the density distribution.

In Fig. 4, the left column shows the contours of the MEAN of the density distribution at space–time point (x, y) in the day-to-day stochastic process at different times. Pedestrians enter the platform from the left entrance, pass through the corridors, and leave through the exit gate. As the width of the corridor is reduced at $x \in [40, 60]$ m, pedestrians tend to avoid the obstacle, resulting in two shocks at $x \in [0, 40]$ m, $y \in [10, 30]$ m and $t = 90$ s. A similar phenomenon is observed before the exit as pedestrians leave the platform at $t = 180$ s. Throughout this period, the density is highest at the four corners of the obstacle and on both sides of the exit. The contour results illustrate the evolution of the congestion pattern of pedestrians and help identify areas with high density. The middle column displays the contours of the SDEV of the density distribution at space–time point (x, y) in the day-to-day stochastic process at different times. In areas expected to exhibit high pedestrian density, the SDEV is also higher. This result indicates that the demand stochasticity has a more notable effect on the higher-density regions of the platform. Specifically, at $t = 120$ and 150 s, the peak position of the SDEV shock around the obstacle always appears behind that of the mean density along the direction of movement. As more pedestrians traverse the platform, the pedestrian density varies within a wide range relative to the average level, which increases the risk of crowding in these shock areas. The statistical information provided by both MEAN and SDEV can assist the evaluation of the obstructed facility and facilitate the development of strategies to improve service in walking environments. The right column displays the risk regions defined in (41) at different times. At these locations, the average density is moderate, but there is large variance, leading to exceptional congestion on critical days that could be overlooked in a standard design process based on the average demand. From this point of view, the walking facility could be designed by increasing the capacity to a maximum value at the locations such that the system works 95% of the time during operation.

These observations are consistent with the theoretical findings in Section 2.2. The two examples considered in Section 2.2 respectively correspond to the processes of pedestrians entering the platform and encountering the obstacle in this numerical example. Initially, when pedestrians are entering the platform, the spreading out of the crowd (rarefaction solution) can be clearly seen, and the MEAN and SDEV of pedestrian density are higher at the tail of the crowd and lower at the head. When the pedestrians encounter the obstacle and congestion (shock solution) occurs, the SDEV reaches a significantly high value at these locations and introduces risk into the system. The lagging of the SDEV peak position behind the MEAN also validates the conclusion from the theoretical analysis.

The lognormal random variable ξ has a 95% confidence interval $[0.82, 1.20]$, satisfying $P(0.82 < \xi < 1.20) \approx 0.95$. For comparison, this study presents the solution obtained from the deterministic model without random inputs using the average demand $q(\boldsymbol{x}, t)$ ($\xi = 1$) and a larger demand scaled up by $\xi = 1.2$, which is the maximum value in the 95% confidence interval of ξ, as indicated in Eq. (38). Figs. 5 and 6 show the pedestrian density along lines $y = 28.5$ m and $y = 32.5$ m, respectively. The label "Deterministic Case" indicates the solution obtained using the deterministic model with $\xi = 1$ and $\xi = 1.2$. Under demand stochasticity, the ME-PCM solution ($N_e = 20, N_p = 3$) varies within a range that has a 95% probability (labeled "95% Confidence Interval"), and its expectation is ME-PCM MEAN. A comparison of the deterministic results reveals that by increasing the demand from $\xi = 1$ to $\xi = 1.2$, the pedestrian density in the facility increases most of the time. However, at $x = 40$ m, $y = 28.5$ m, $t = 120$ s near the obstacle, the density obtained using the model with random inputs is much higher than that in the deterministic case ($\xi = 1.2$). A reasonable explanation is that in a stochastic environment, the congestion occurs at different locations, as explained in the foregoing theoretical analysis. This shows that to calculate the range of pedestrian density variation, the deterministic model cannot only simulate a few samples by simply increasing the traffic demand at the entrance; rather, it needs more samples with different deterministic inputs. In contrast, the ME-PCM solution can capture density variations influenced by demand stochasticity and identify risk regions much more efficiently. Moreover, at $y = 32.5$ m, $t = 150$ s, and 180 s, the results of ME-PCM MEAN are considerably different from the deterministic results with averaged demand ($\xi = 1$), which further validates the effectiveness of considering the demand stochasticity. In the figure, the 95% confidence interval indicates that the pedestrian density may appreciably exceed its average level at specific locations on the platform under extreme conditions, such as at $x = 55$ m, $y = 32.5$ m, and $t = 150$ s. This information can facilitate the evaluation of the traffic facility, as congestion is more likely to occur at these locations.

Fig. 7 shows the variations in Total_{ρ} and Total_{σ} over the simulation period, where Total_{ρ} and Total_{σ} respectively denote the total MEAN and SDEV of the density over the entire spatial space defined in (40). The maximum Total_{ρ} occurs near $t = 110$ s, preceding the moment when the average traffic demand (38) decreases to zero, i.e., $t = 120$ s. This early peak in Total_{ρ} is attributable to the departure of the first batch of pedestrians entering the platform. In addition, as pedestrians walk by the obstacle and exit the gate,

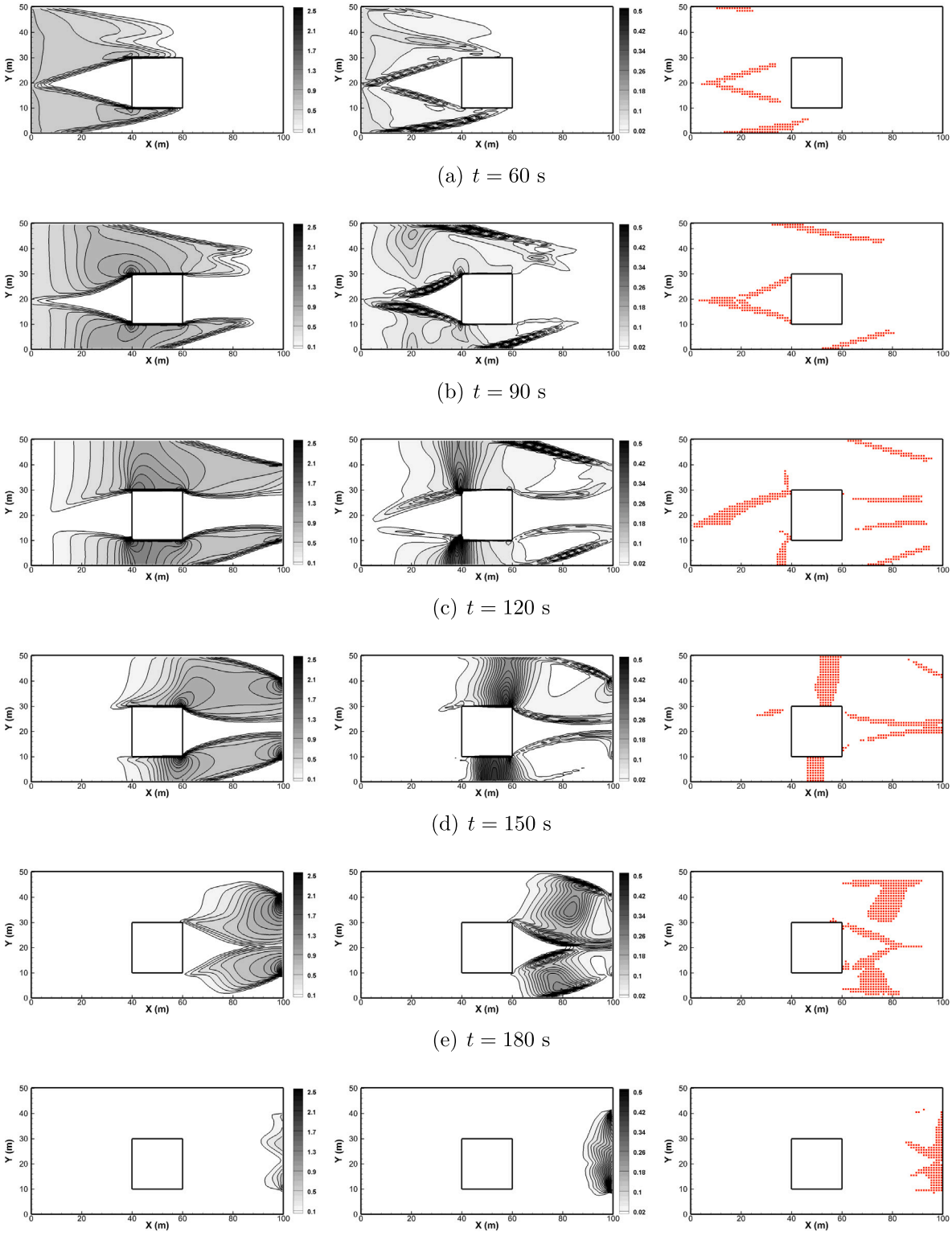

Fig. 4. Density contour plot of MEAN and SDEV at different times in case 1 using ME-PCM with $N_e = 20$ random elements and $N_p = 3$ polynomial basis. Left: MEAN. Middle: SDEV. Right: risk region.

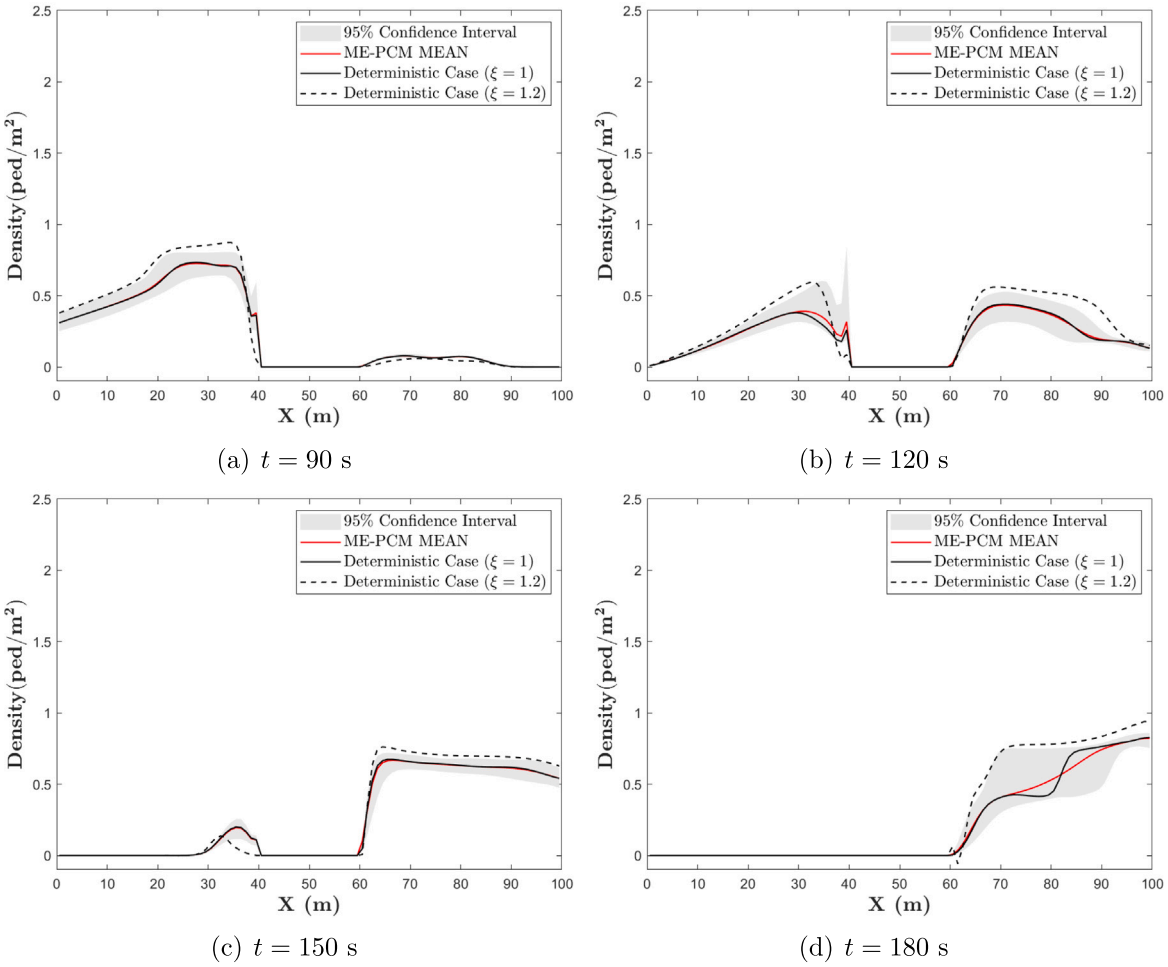

Fig. 5. The pedestrian density distribution along line $y = 28.5$ m.

Total_ρ begins to decrease, whereas Total_σ decreases at a later time and at a lower rate. This observation, which is consistent with the analytical result, shows that in narrow regions of the walking facility, considerable time (approximately 80 s) is required to eliminate the effects of high variance caused by congestion.

Next, this study examines the convergence performance of the ME-PCM against the performances of several commonly used approaches, namely the gPC, MC, and quasi-MC (QMC). The classical gPC corresponds to a special case of the ME-PCM with only one random element; i.e., $N_e = 1$. Considering a specific space–time point near the obstacle ($x = 40$ m, $y = 30$ m, $t = 120$ s), the solution response to the random input is simulated in the interval $\xi \in [0.6, 1.6]$, as depicted in Fig. 8(a). When ξ is small, the pedestrian density at the specific location is almost zero. However, at higher ξ (ranging approximately from 1.1 to 1.5), there is a congestion shock at this location, leading to a rapid increase in pedestrian density. If the gPC method uses global basis functions to represent the solution, as the polynomial order N_p increases, the approximate solution obtained by the gPC method converges gradually, and the error becomes appreciable on both sides of the interval. However, it is not necessary to use a large number of polynomial basis functions because the orthogonal basis can locally represent the solution when using the ME-PCM. Fig. 8(b) shows the results of the ME-PCM with $N_e = 1, 3, 5$ elements. Notably, improved convergence is observed even when only three basis functions are used. This flexibility is advantageous, as it avoids potential problems associated with high-degree polynomials. Moreover, the ME-PCM provides users with two pathways to improve accuracy, enabling the selection of a more suitable pair of N_e and N_p.

The ME-PCM results are next compared with the MC and QMC results. Fig. 9 presents the RRMSE of the MEAN and SDEV for the MC and QMC methods, where N is the number of samples and E_ρ and E_σ are obtained using (39). Adopting a first-order polynomial to approximate the error in a least-squares sense, the accuracy of the MC method is obtained as $O(N^{-0.36})$ and $O(N^{-0.44})$ for MEAN and SDEV, respectively. In the same manner, the accuracy of the QMC method is obtained as $O(N^{-0.83})$ for MEAN and $O(N^{-0.76})$ for SDEV. Note that the expected rates are $O(N^{-\frac{1}{2}})$ for the MC method and $O(N^{-1})$ for the QMC method. In Fig. 10, the errors of the ME-PCM are plotted for $N_p = 1, 2, 3$. From the least-square fitted line, the convergence rates are approximated for the cases (i)

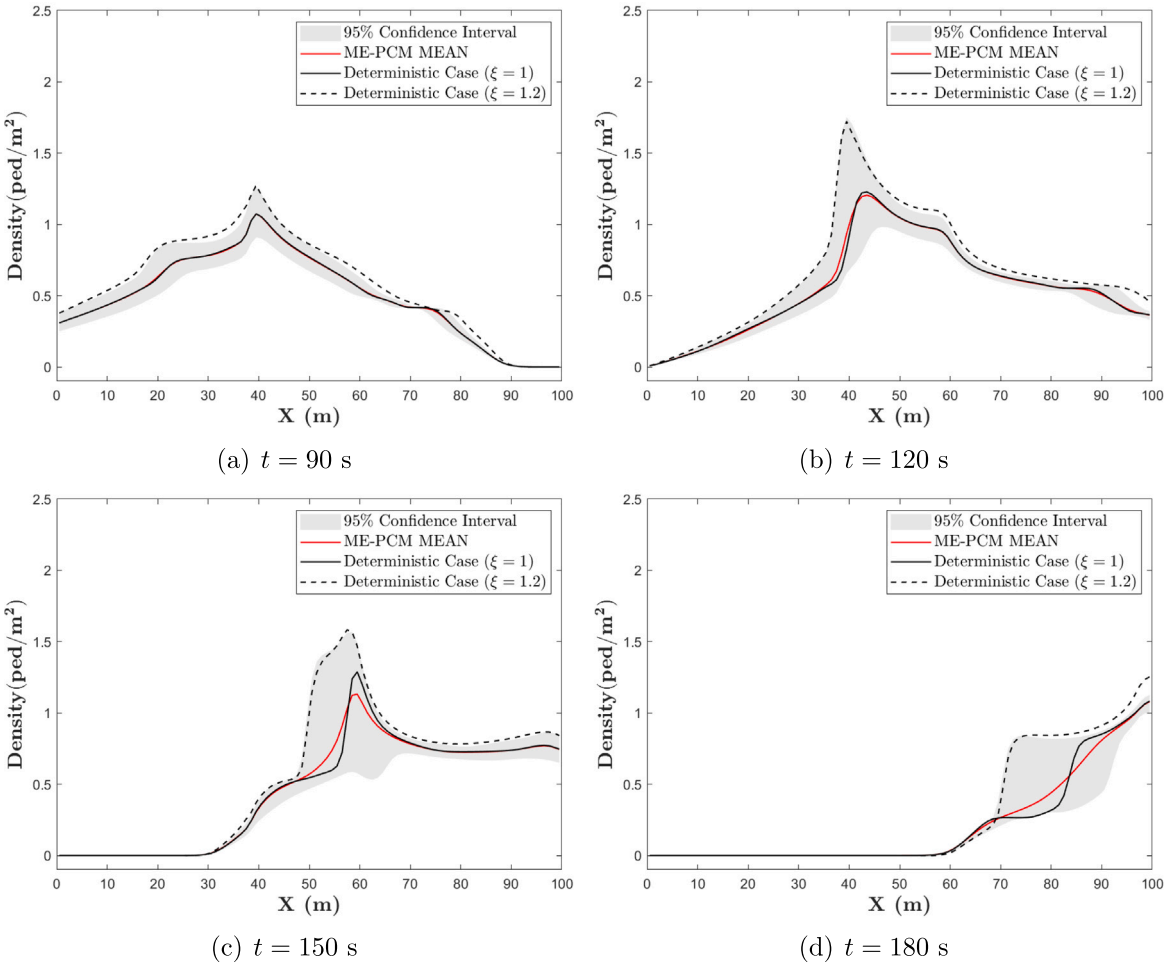

Fig. 6. The pedestrian density distribution along line $y = 32.5$ m.

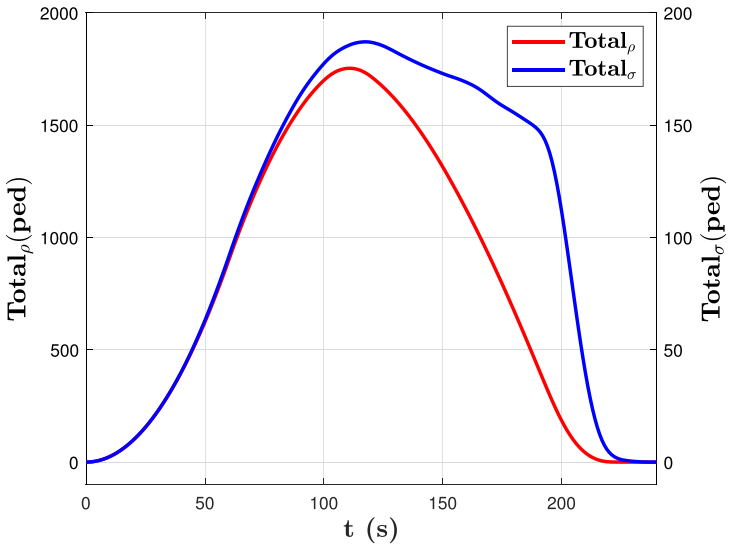

Fig. 7. The variations in total MEAN and SDEV with respect to time t.

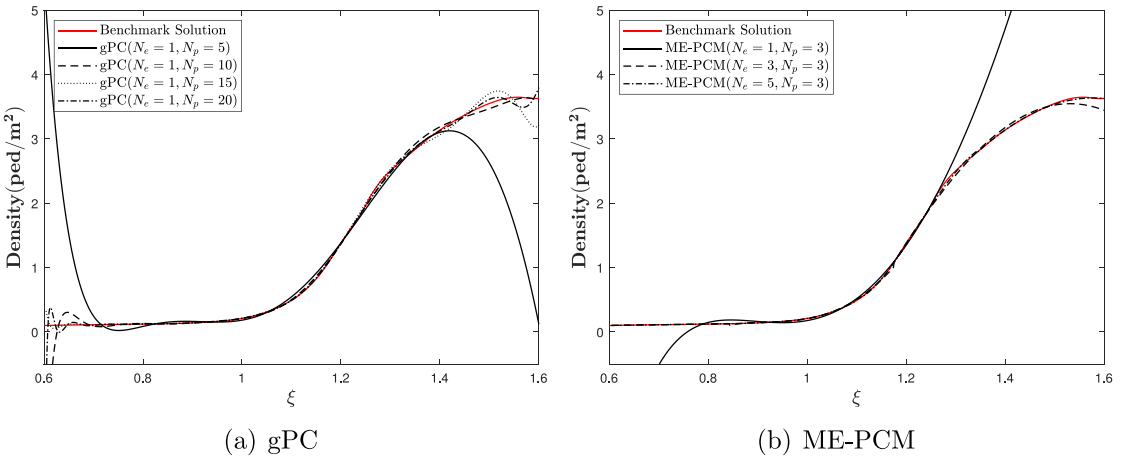

Fig. 8. Comparison between gPC and ME-PCM.

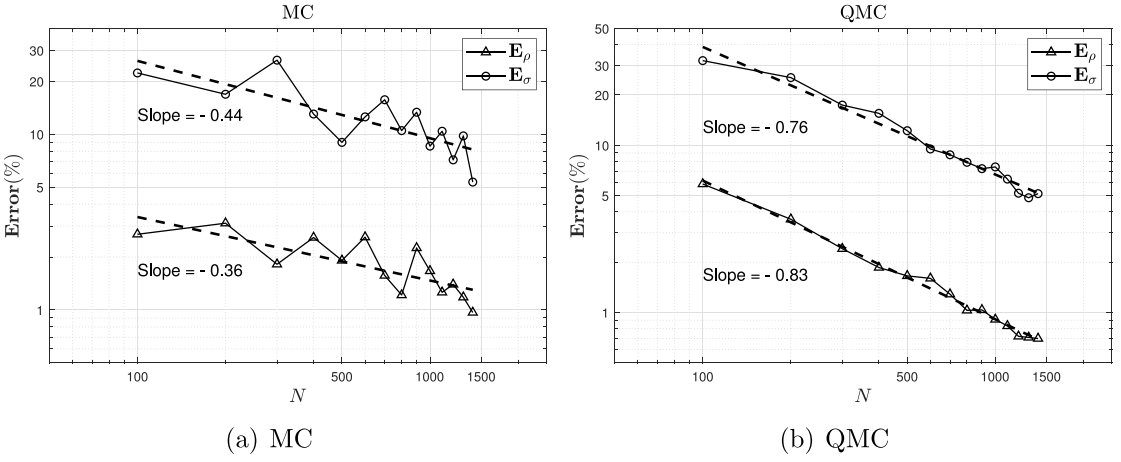

Fig. 9. Convergence of MC and QMC.

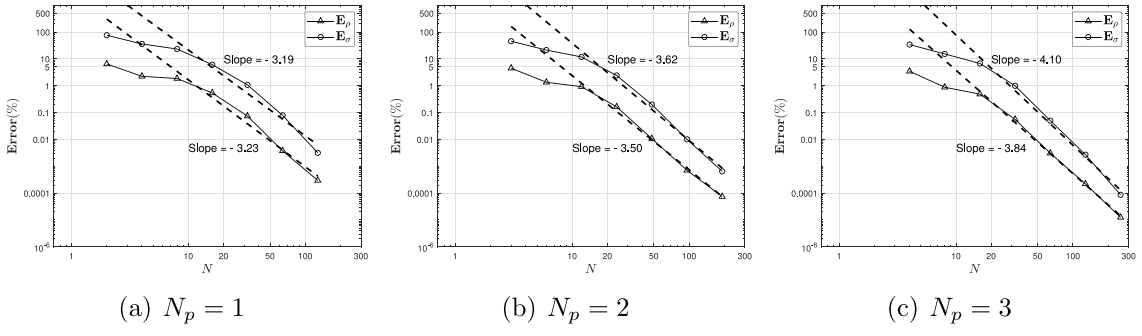

Fig. 10. Convergence comparisons of ME-PCM with $N_p = 1, 2, 3$.

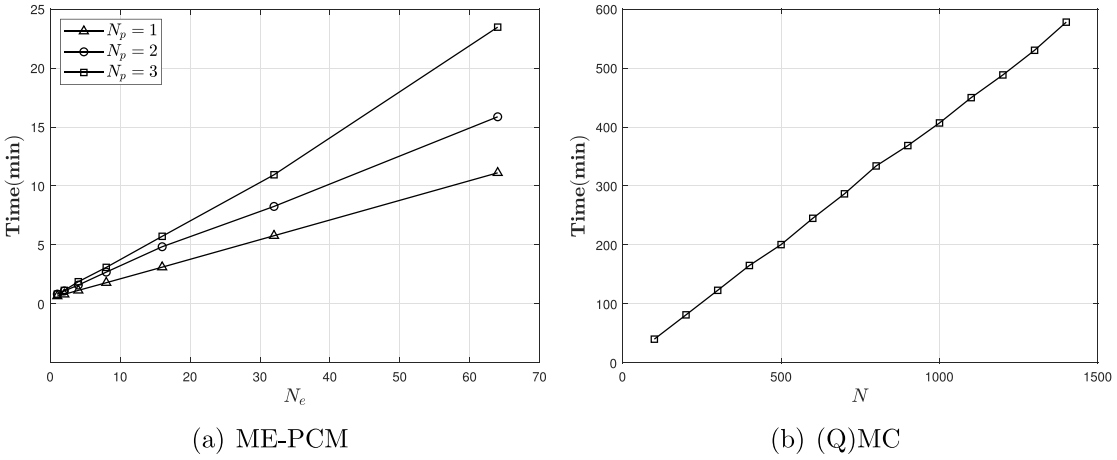

Fig. 11. Comparison of computational cost. Left: simulation time with respect to the number of random elements N_e with $N_p = 1, 2, 3$. Right: simulation time with respect to the number of (Q)MC samples N.

Table 1
Comparison of estimated number of samples required to achieve the MEAN error ϵ_{tol} by different approaches in case 1.

MEAN					
ϵ_{tol}	ME-PCM			MC	QMC
	$N_p = 1$	$N_p = 2$	$N_p = 3$		
1%	12	13	14	2908	893
0.1%	24	25	25	1,702,026	14,327
0.001%	99	92	85	$>10^{11}$	3,685,905

Table 2
Comparison of estimated number of samples required to achieve the SDEV error ϵ_{tol} by different approaches in case 1.

SDEV					
ϵ_{tol}	ME-PCM			MC	QMC
	$N_p = 1$	$N_p = 2$	$N_p = 3$		
1%	26	27	29	166,008	12,076
0.1%	54	52	51	31,039,808	247,050
0.001%	226	184	155	$>10^{12}$	$>10^{8}$

$N_p = 1$: $O(N^{-3.23})$ and $O(N^{-3.19})$), (ii) $N_p = 2$: $O(N^{-3.50})$ and $O(N^{-3.62})$), and (iii) $N_p = 3$: $O(N^{-3.84})$ and $O(N^{-4.10})$), for the MEAN and SDEV. The accuracy does not achieve the optimal order $O(N^{-2(N_p+1)})$ as the solution involves shocks without enough regularity. However, it is observed that the ME-PCM converges much more rapidly than the MC and QMC methods, and the convergence rate increases with the polynomial order N_p.

As a sampling-based method, the ME-PCM has a computational cost that is mainly determined by the number of sample points $N = (N_p + 1)N_e$, because the cost of basis construction can be neglected. Fig. 11(a) shows the computational times for different polynomial orders with respect to the number of random elements N_e. For the same N_e, the cost increases with the polynomial order N_p, as N_p+1 sample points are simulated for an N_p degree polynomial in each element. The (Q)MC time cost is plotted for different sizes of (Q)MC samples in Fig. 11(b). Although the MC method robustly simulates the solution distribution, the computation cost is extremely high. Each sample has a computational cost of approximately 0.4 min in this example.

To further illustrate the efficiency of the ME-PCM, its speedup performance is calculated relative to the MC and QMC methods. The number of simulated samples can be used to quantify the speedup. Using the least-square fitted lines in Figs. 9 and 10, the estimated number of samples required to achieve a tolerance error ϵ_{tol} is calculated for the ME-PCM and MC and QMC methods, as given in Tables 1 and 2. The number of samples required to achieve a desired accuracy is notably higher for the MC and QMC methods than for the ME-PCM. Furthermore, it is observed that the ME-PCM with $N_p = 3$ outperforms the ME-PCM with $N_p = 1, 2$ in achieving a higher accuracy of 0.001%. Although parallelization can be considered both for the ME-PCM procedure and robust Monte Carlo methods, it is not used in this example. To compare efficiency, the test conditions are kept the same without parallelization. Due to the fast convergence of the ME-PCM, only a few samples are actually required to achieve a small error (1%, an acceptable value), so the superiority of parallelism for the ME-PCM in this example is not obvious. Parallelization is recommended if users find that more samples are required to meet the desired tolerance error for their problem.

Table 3
Comparison of convergence order of different approaches in case 2.

Order	ME-PCM			MC	QMC
	$N_p = 1$	$N_p = 2$	$N_p = 3$		
MEAN	2.46	2.95	3.09	0.35	1.00
SDEV	2.18	2.64	2.82	0.27	0.79

Table 4
Comparison of estimated number of samples required to achieve the MEAN error ϵ_{tol} by different approaches in case 2.

MEAN					
ϵ_{tol}	ME-PCM			MC	QMC
	$N_p = 1$	$N_p = 2$	$N_p = 3$		
1%	19	21	23	4469	880
0.1%	49	47	48	3,075,132	8623
0.001%	316	222	214	$>10^{12}$	826,218

Table 5
Comparison of estimated number of samples required to achieve the SDEV error ϵ_{tol} by different approaches in case 2.

SDEV					
ϵ_{tol}	ME-PCM			MC	QMC
	$N_p = 1$	$N_p = 2$	$N_p = 3$		
1%	44	43	45	17,607,957	11,651
0.1%	127	102	101	$>10^{10}$	214,314
0.001%	1048	580	518	$>10^{18}$	72,502,420

3.4.2. Case 2: $\xi \sim Lognormal(1.0, 0.2^2)$

In this test case, $\xi \sim \text{Lognormal}(1.0, 0.2^2)$ with a larger variance. Fig. 12 displays the MEAN and SDEV of the density distribution and the risk region at different times. It is seen that the MEAN is similar to that in case 1, whereas the SDEV tends to be higher, as expected. As a result, the risk region mainly distributed in pedestrian-congested areas, becomes wider.

The convergence rates when using the different approaches are summarized in Table 3. Compared with the results in case 1, the ME-PCM has a lower convergence rate but still performs better than the MC and QMC methods. Tables 4 and 5 present the speedup results. When using the same numbers of random elements and polynomial basis functions, the number of samples required to achieve error ϵ_{tol} is larger than that in case 1. This observation is reasonable, as a larger variance leads to a broader range of traffic demand, resulting in a larger error in the stochastic moment statistics of pedestrian density. Nevertheless, an excellent speedup performance is maintained, indicating that the ME-PCM algorithm is robust and can be applied to similar problems.

4. Conclusion

Based on dynamic continuum models, some analytical results pertaining to the effect of random inputs on pedestrian flow propagation were first presented. For a general model that can be expressed as sets of PDEs with random inputs, the ME-PCM solver, used in uncertainty quantification, was employed to efficiently derive the solution and its statistical properties. The algorithm application procedure, including decomposition, sampling, and reconstruction steps, was given. In a demonstration case, this study considered demand stochasticity by randomizing the inflow boundary condition of Hughes model. A two-dimensional numerical example of a corridor with an obstacle was simulated, and two variance cases were considered. The pedestrian density distribution was accurately derived using the ME-PCM, with a notably reduced computational cost. From the ME-PCM solutions, statistical information was accurately obtained for the evaluation of walking facilities at risk of exceptional congestion. In a comparison with the MC and QMC methods, the ME-PCM had a better convergence rate, although there was shock during the simulation period. The ME-PCM also required fewer samples to achieve a desired tolerance error. In a successful application of the spectral method to quantify the uncertainty in pedestrian traffic flow models, this study showed the ability of the ME-PCM to investigate other traffic models involving randomized parameters without limitations on governing PDEs and numerical schemes.

This study considered only a single random variable. The ME-PCM will be developed to handle pedestrian models with more random inputs in future work. Other considerations, such as randomizing the parameters in speed-density relations, also have practical importance.

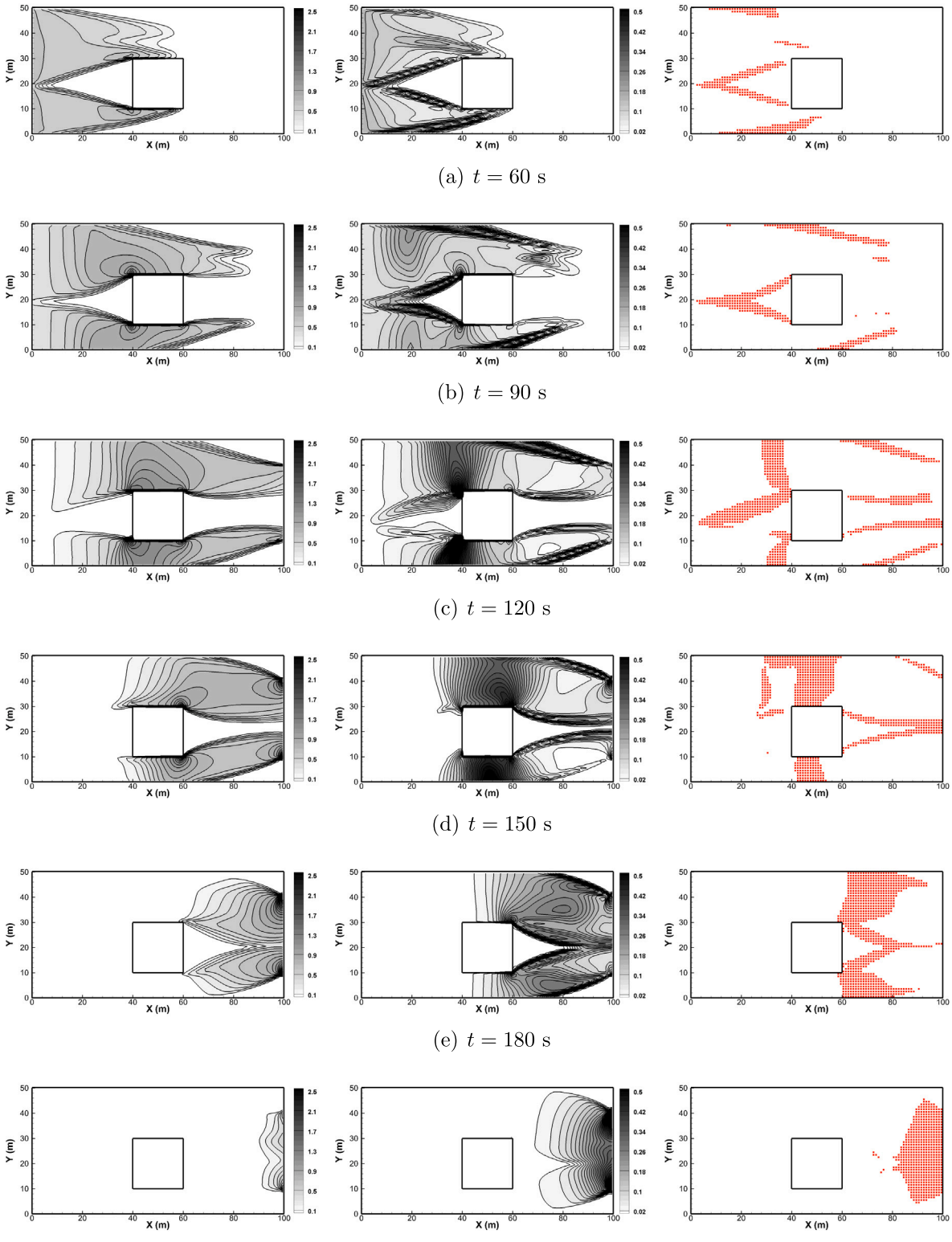

Fig. 12. Density contour plot of MEAN and SDEV at different times in case 2 using ME-PCM with $N_e = 20$ random elements and $N_p = 3$ polynomial basis. Left: MEAN. Middle: SDEV. Right: risk region.

CRediT authorship contribution statement

Zepeng Liu: Writing – review & editing, Writing – original draft, Visualization, Validation, Methodology, Formal analysis, Data curation, Conceptualization. **S.C. Wong:** Writing – review & editing, Writing – original draft, Validation, Supervision, Resources, Project administration, Methodology, Funding acquisition, Conceptualization. **Liangze Yang:** Conceptualization, Data curation, Formal analysis, Methodology, Validation, Visualization, Writing – original draft, Writing – review & editing. **Chi-Wang Shu:** Writing – review & editing, Writing – original draft, Supervision, Methodology, Conceptualization. **Mengping Zhang:** Writing – review & editing, Writing – original draft, Supervision, Methodology, Conceptualization.

Acknowledgments

The work described in this paper was supported by grants from the Research Grants Council of the Hong Kong Special Administrative Region, China (Project Nos. 17204919 and 17202223). The second author was supported by the Francis S Y Bong Professorship in Engineering, the third author was supported by National Natural Science Foundation of China grant 12401477, the fourth author was supported by National Science Foundation grant DMS-2309249, and the fifth author was supported by National Natural Science Foundation of China grant 12271499.

References

Barreiro-Gomez, J., Masmoudi, N., 2023. Differential games for crowd dynamics and applications. Math. Models Methods Appl. Sci. 33 (13), 2703–2742.
Brilon, W., Geistefeldt, J., Regler, M., 2005. Reliability of freeway traffic flow: a stochastic concept of capacity. In: Proceedings of the 16th International Symposium on Transportation and Traffic Theory. Vol. 125143, Citeseer.
Burger, M., Di Francesco, M., Markowich, P., Wolfram, M.-T., 2013. Mean field games with nonlinear mobilities in pedestrian dynamics. arXiv preprint arXiv:1304.5201.
Caflisch, R.E., 1998. Monte Carlo and quasi-Monte Carlo methods. Acta Numer. 7, 1–49.
Cameron, R.H., Martin, W.T., 1947. The orthogonal development of non-linear functionals in series of Fourier-Hermite functionals. Ann. Math. 385–392.
Cao, K., Chen, Y., Stuart, D., Yue, D., 2015. Cyber-physical modeling and control of crowd of pedestrians: a review and new framework. IEEE/ CAA J. Autom. Sin. 2 (3), 334–344.
Cheng, M., Hou, T.Y., Zhang, Z., 2013a. A dynamically bi-orthogonal method for time-dependent stochastic partial differential equations I: derivation and algorithms. J. Comput. Phys. 242, 843–868.
Cheng, M., Hou, T.Y., Zhang, Z., 2013b. A dynamically bi-orthogonal method for time-dependent stochastic partial differential equations II: adaptivity and generalizations. J. Comput. Phys. 242, 753–776.
Cho, H., Venturi, D., Karniadakis, G.E., 2014. Statistical analysis and simulation of random shocks in stochastic Burgers equation. Proc. R. Soc. A: Math. Phys. Eng. Sci. 470 (2171), 20140080.
Chung, E., Ohtani, O., Kuwahara, M., 2005. Effect of rainfall on travel time and travel demand. In: 5th ITS European Congress, Hannover, Germany.
Djehiche, B., Tcheukam, A., Tembine, H., 2017. A mean-field game of evacuation in multilevel building. IEEE Trans. Autom. Control 62 (10), 5154–5169.
Dogbé, C., 2010. Modeling crowd dynamics by the mean-field limit approach. Math. Comput. Modelling 52 (9–10), 1506–1520.
Fan, T., Wong, S.C., Zhang, Z., Du, J., 2023. A dynamically bi-orthogonal solution method for a stochastic Lighthill-Whitham-Richards traffic flow model. Computer- Aided Civ. Infrastruct. Eng. 38 (11), 1447–1461.
Foo, J., Wan, X., Karniadakis, G.E., 2008. The multi-element probabilistic collocation method (ME-PCM): error analysis and applications. J. Comput. Phys. 227 (22), 9572–9595.
Gautschi, W., 1982. On generating orthogonal polynomials. SIAM J. Sci. Stat. Comput. 3 (3), 289–317.
Gerritsma, M., Van der Steen, J.-B., Vos, P., Karniadakis, G., 2010. Time-dependent generalized polynomial chaos. J. Comput. Phys. 229 (22), 8333–8363.
Ghanem, R., Red-Horse, J., 1999. Propagation of probabilistic uncertainty in complex physical systems using a stochastic finite element approach. Phys. D: Nonlinear Phenom. 133 (1–4), 137–144.
Ghanem, R.G., Spanos, P.D., 2003. Stochastic Finite Elements: A Spectral Approach. Courier Corporation.
Ghattassi, M., Masmoudi, N., 2023. Non-separable mean field games for pedestrian flow: generalized Hughes model. arXiv preprint arXiv:2310.04702.
Giles, M.B., 2015. Multilevel Monte Carlo methods. Acta Numer. 24, 259–328.
Hoogendoorn, S.P., Bovy, P.H., 2004. Dynamic user-optimal assignment in continuous time and space. Transp. Res. Part B: Methodol. 38 (7), 571–592.
Huang, L., Wong, S.C., Zhang, M., Shu, C.-W., Lam, W.H.K., 2009a. Revisiting Hughes' dynamic continuum model for pedestrian flow and the development of an efficient solution algorithm. Transp. Res. Part B: Methodol. 43 (1), 127–141.
Huang, L., Xia, Y., Wong, S., Shu, C.-W., Zhang, M., Lam, W., 2009b. Dynamic continuum model for bi-directional pedestrian flows. Proc. Inst. Civ. Engineers-Eng. Comput. Mech. 162 (2), 67–75.
Hughes, R.L., 2002. A continuum theory for the flow of pedestrians. Transp. Res. Part B 36 (6), 507–535.
Jabari, S.E., Zheng, J., Liu, H.X., 2014. A probabilistic stationary speed–density relation based on Newell's simplified car-following model. Transp. Res. Part B: Methodol. 68, 205–223.
Jiang, Y.-Q., Liu, R.-X., Duan, Y.-L., 2011. Numerical simulation of pedestrian flow past a circular obstruction. Acta Mech. Sin. 27 (2), 215–221.
Jiang, G.-S., Shu, C.-W., 1996. Efficient implementation of weighted ENO schemes. J. Comput. Phys. 126 (1), 202–228.
Kerner, B.S., Klenov, S.L., 2006. Probabilistic breakdown phenomenon at on-ramp bottlenecks in three-phase traffic theory: congestion nucleation in spatially non-homogeneous traffic. Phys. A 364, 473–492.
Kesting, A., Treiber, M., Helbing, D., 2010. Enhanced intelligent driver model to access the impact of driving strategies on traffic capacity. Philos. Trans. R. Soc. A: Math. Phys. Eng. Sci. 368 (1928), 4585–4605.
Kincaid, D.R., Cheney, E.W., 2009. Numerical Analysis: Mathematics of Scientific Computing. Vol. 2, American Mathematical Society..
Lachapelle, A., Wolfram, M.-T., 2011. On a mean field game approach modeling congestion and aversion in pedestrian crowds. Transp. Res. Part B: Methodol. 45 (10), 1572–1589.
LeVeque, R.J., 1992. Numerical methods for conservation laws. Vol. 214, Springer.
Li, J., Chen, Q.Y., Wang, H., Ni, D., 2012. Analysis of LWR model with fundamental diagram subject to uncertainties. Transp. 8 (6), 387–405.
Liang, H., Du, J., Wong, S.C., 2021. A continuum model for pedestrian flow with explicit consideration of crowd force and panic effects. Transp. Res. Part B: Methodol. 149, 100–117.
Newell, G.F., 1961. Nonlinear effects in the dynamics of car following. Oper. Res. 9 (2), 209–229.

Parisi, D.R., Sartorio, A.G., Colonnello, J.R., Garcimartín, A., Pugnaloni, L.A., Zuriguel, I., 2021. Pedestrian dynamics at the running of the bulls evidence an inaccessible region in the fundamental diagram. Proc. Natl. Acad. Sci. USA 118 (50), e2107827118.
Parry, K., Hazelton, M.L., 2013. Bayesian inference for day-to-day dynamic traffic models. Transp. Res. Part B: Methodol. 50, 104–115.
Ramírez, M., Torres, F., Toledo, B., Coello, M., Correa-Burrows, P., Rogan, J., Valdivia, J., 2019. Unpredictability in pedestrian flow: the impact of stochasticity and anxiety in the event of an emergency. Phys. A 531, 121742.
Sayegh, A.S., Connors, R.D., Tate, J.E., 2018. Uncertainty propagation from the cell transmission traffic flow model to emission predictions: a data-driven approach. Transp. Sci. 52 (6), 1327–1346.
Schwab, C., Tokareva, S., 2013. High order approximation of probabilistic shock profiles in hyperbolic conservation laws with uncertain initial data. ESAIM Math. Model. Numer. Anal. 47 (3), 807–835.
Shu, C.-W., Osher, S., 1988. Efficient implementation of essentially non-oscillatory shock-capturing schemes. J. Comput. Phys. 77 (2), 439–471.
Sumalee, A., Uchida, K., Lam, W.H.K., 2011a. Stochastic multi-modal transport network under demand uncertainties and adverse weather condition. Transp. Res. Part C: Emerg. Technol. 19 (2), 338–350.
Sumalee, A., Zhong, R.X., Pan, T.L., Szeto, W.Y., 2011b. Stochastic cell transmission model (SCTM): a stochastic dynamic traffic model for traffic state surveillance and assignment. Transp. Res. Part B 45 (3), 507–533.
Tordeux, A., Schadschneider, A., 2016. White and relaxed noises in optimal velocity models for pedestrian flow with stop-and-go waves. J. Phys. A 49 (18), 185101.
Twarogowska, M., Goatin, P., Duvigneau, R., 2014. Macroscopic modeling and simulations of room evacuation. Appl. Math. Model. 38 (24), 5781–5795.
Wan, X., Karniadakis, G.E., 2005. An adaptive multi-element generalized polynomial chaos method for stochastic differential equations. J. Comput. Phys. 209 (2), 617–642.
Wan, X., Karniadakis, G.E., 2006. Multi-element generalized polynomial chaos for arbitrary probability measures. SIAM J. Sci. Comput. 28 (3), 901–928.
Wang, Y., Papageorgiou, M., 2005. Real-time freeway traffic state estimation based on extended Kalman filter: a general approach. Transp. Res. Part B: Methodol. 39 (2), 141–167.
Wiener, N., 1938. The homogeneous chaos. Amer. J. Math. 60 (4), 897–936.
Wong, S.C., Leung, W.L., Chan, S.H., Lam, W.H.K., Yung, N.H.C., Liu, C.Y., Zhang, P., 2010. Bidirectional pedestrian stream model with oblique intersecting angle. J. Transp. Eng. 136 (3), 234–242.
Xia, Y., Wong, S., Shu, C.-W., 2009. Dynamic continuum pedestrian flow model with memory effect. Phys. Rev. E 79 (6), 066113.
Xiu, D., 2009. Fast numerical methods for stochastic computations: a review. Commun. Comput. Phys. 5 (2–4), 242–272.
Xiu, D., Karniadakis, G.E., 2002. The Wiener–Askey polynomial chaos for stochastic differential equations. SIAM J. Sci. Comput. 24 (2), 619–644.
Zhang, Y.-T., Zhao, H.-K., Qian, J., 2006. High order fast sweeping methods for static Hamilton–Jacobi equations. J. Sci. Comput. 29, 25–56.
Zhong, X., Shu, C.-W., 2022. Entropy stable Galerkin methods with suitable quadrature rules for hyperbolic systems with random inputs. J. Sci. Comput. 92 (1), 14.
Zhong, R.X., Sumalee, A., Pan, T.L., Lam, W.H.K., 2013. Stochastic cell transmission model for traffic network with demand and supply uncertainties. Transp. A: Transp. Sci. 9 (7), 567–602.